previously unreported 2^+ level in addition to the well known 1^- level. (2) The 13.88-MeV level has a spin and parity of 4^+. (3) The previously unreported level at 14.80 MeV is either 0^+ or 1^-. The simultaneous experiment by Ferguson[17,18] yielded nearly identical results.

Several general features of the coupled-equations approach are well illustrated by the $C^{12}(\alpha,\alpha_1)C^{12*}$ reaction. DWBA overestimates the cross section by more than an order of magnitude at these energies (this is no longer true at higher energies). The coupling of additional states has a pronounced effect on the elastic scattering, even when the inelastic cross section is small. Many of the qualitative features of the experimental data (shape, magnitude, energy dependence) are correctly reproduced. Explicit consideration of only two channels, and compound nuclear effects preclude detailed quantitative agreement. Compared to DWBA, however, the "two-channel" coupled-equations approximation is fairly successful.

ACKNOWLEDGMENTS

The authors would like to thank Dr. W. E. Hunt, Dr. M. K. Mehta, J. D. Marshall, and J. B. Seaborn for assistance in performing the experiment; S. Brudno for aid in the computing performed at Florida State University; and Dr. S. Edwards, Dr. N. R. Fletcher, Dr. J. D. Fox and Dr. J. W. Nelson for valuable discussions.

One of us (G.E.M.) would like to thank the Oak Ridge Institute of Nuclear Studies for financial assistance; Dr. B. Buck for the use of his computer programs; D. E. Arnurius for assistance with the computing performed at Oak Ridge; and Dr. Buck and Dr. G. R. Satchler for numerous invaluable discussions.

PHYSICAL REVIEW VOLUME 133, NUMBER 6B 23 MARCH 1964

Double Stripping: (He^3,n) Reaction*

ERNEST M. HENLEY AND DAVID U. L. YU
University of Washington, Seattle, Washington
(Received 6 November 1963)

The two-nucleon stripping reaction is examined in detail, with particular reference to the (He^3,n) reaction. Three models are studied and compared: (1) the plane-wave Born approximation, (2) the distorted-wave Born approximation, and (3) a simple diffraction model. Zero-range approximations are not assumed *a priori*. For (1) and (2), the wave functions of the two captured nucleons are taken to be eigenstates of an infinite harmonic oscillator, the strength of which is adjusted to reproduce single-particle eigenfunctions of a finite Saxon well in regions close to the nuclear surface. The first model is primarily employed to show that the modulation of the angular distribution due to the structure of He^3 is also sensitive to the form and range of the stripping interaction. Model (2) is used to calculate absolute differential cross sections to various final states, in particular for C^{12}, O^{16}, Ni, and Sn targets with 20-MeV incident He^3 ions. Comparison with experimental data is made where available and agreement is found. To further such comparisons we also compute summed cross sections to several low-lying states of the final nucleus. Spectroscopic weights are obtained for pure and mixed configurations of single-particle wave functions. Model (3) provides insight into the dominant features of the experimental and calculated [model (2)] differential cross sections. These are: (a) a strong forward peaking of the distribution especially for spin 0 to 0 transitions, but also for summed cross sections, (b) an angular distribution for such sums that is roughly independent of the atomic weight of the target nucleus, and (c) an enhancement of cross sections to higher spin states ($\approx$3 or 4) of final nuclei. These features are not reproduced with model (1).

I. INTRODUCTION

THE use of deuteron projectiles for studying nuclear spectroscopy is well known. Recently, attention has focused on the double stripping reaction for the same purpose. In fact, it has been pointed out by Yoshida[1] that double stripping may be particularly suited to the study of collective (vibrational) levels.

Although considerable experimental investigation of the two-nucleon stripping reaction has already taken place, all theoretical analyses to date use the plane-wave Born approximation to describe the process. This, even though not valid, is of some use for obtaining level spin assignments from angular distribution in deuteron stripping. However, it is not known whether the same information can be extracted from the application of the Born approximation to two-nucleon stripping processes.

In this paper we shall examine the two-nucleon stripping reaction in detail. In Sec. II we first develop a general formulation of the double-stripping reaction, which we specialize to the (He^3,n) process as a particular example. We do not make any zero-range approximations. We use a Gaussian for the internal wave function of He^3 as well as for the stripping interaction. For the

* Supported in part by the U. S. Atomic Energy Commission under Contract A. T. (45-1)1388, Program B.
[1] S. Yoshida, Nucl. Phys. **33**, 685 (1962).

captured nucleons [two protons in the (He^3,n) reaction] we employ shell-model wave functions of an infinite harmonic oscillator. The use of this potential for bound states allows a separation of center-of-mass and relative coordinates.

We first reexamine the plane-wave Born approximation description of the (He^3,n) reaction in order to bring out some features not studied previously, such as those involving the stripping interaction. Thus, we show that the "He^3 form factor," which limits the magnitude of the differential cross section at large angles, is sensitive to the form and range of this interaction. However for medium energies, we demonstrate that this factor, akin to that which occurs in the Born approximation of deuteron stripping, is unimportant in the forward hemisphere. At higher energies we show that this factor is closely related to the Serber description[2] of the stripping process.

In the last part of Sec. II we fully develop the distorted-wave Born approximation description of the two-nucleon stripping reaction, making use of optical potentials in the incoming and outgoing channels. This model is applied in Sec. III to studies of the (He^3,n) reaction for various targets and to different final states. The spectroscopic amplitudes to these states are computed for pure- and mixed-configuration shell-model wave functions, as well as for the "pairing plus long-range force" model of the Copenhagen group, where applicable. Differential cross sections for 20-MeV He^3 particles are calculated and compared with experiments. Furthermore, in order to make comparisons with threshold detector experiments, we sum the cross sections to low-lying states of the final nucleus. One advantage of this type of experiment is that results obtained therefrom are less sensitive to nuclear spectroscopy and more so to other factors, such as nuclear distortions of the He^3 and neutron. Indeed, Manley[3] finds that a strong forward peaking always obtains for targets at or near closed proton shells[3a]; we show that the distorted-wave Born approximation can explain this characteristic feature.

In the last section we develop a simple diffraction model for the stripping process. This model is based on the strong absorption of the incident He^3 and fairly large absorption of the outgoing neutron in the energy region of interest. It gives insight into the differential cross section of the stripping reaction, particularly the observed forward peaking.

II. FORMULATION

A. Introduction

The Hamiltonian for the interaction of an incident N-nucleon system with a nucleus of mass number A can be written as

$$H=\sum_{k=1}^{A+N} T_k+\sum_{j=1}^{A+N}\sum_{k=j+1}^{A+N} V_{jk}, \tag{1}$$

where T_k is the kinetic energy of nucleon k, and V_{jk} represents a nucleon-nucleon (including Coulomb) interaction. When the incident N-particle system and target nucleus are far apart, the initial wave function Φ_i is an eigenfunction of H_i, ($\hbar=c=1$)

$$H_i=\sum_{k=1}^{A+N} T_k+\sum_{j=1}^{N}\sum_{k=j+1}^{N} V_{jk}+\sum_{j=1}^{A}\sum_{k=j+1}^{A} V_{jk} \tag{2a}$$

of the form (in the laboratory system)

$$\Phi_i=\psi_i(1,\cdots,A)\psi_i'(1,\cdots,N)e^{i\mathbf{P}_N\cdot\mathbf{R}_N}, \tag{2b}$$

where $\psi_i(1,\cdots,A)$ is the internal (isospin-spin-space) wave function of the target and $\psi_i'(1,\cdots,N)$ is that of the incident system. The total momentum $\mathbf{P}_N$ and center-of-mass coordinate $\mathbf{R}_N$ refer to the incident N-body system. For a two-particle stripping reaction the final wave function for the separated system is an eigenfunction of the Hamiltonian H_f,

$$H_f=\sum_{k=1}^{A+N} T_k+\sum_{j=1}^{N-2}\sum_{k=j+1}^{N-2} V_{jk}+\sum_{j=1}^{A+2}\sum_{k=j+1}^{A+2} V_{jk}, \tag{3a}$$

of the form (in the laboratory system)

$$_f=\psi_f(1,\cdots,A+2)\psi_f'(1,\cdots,N-2)\times e^{i\mathbf{P}_{N-2}\cdot\mathbf{R}_{N-2}}e^{i\mathbf{P}_{A+2}\cdot\mathbf{R}_{A+2}}, \tag{3b}$$

where the notation is similar to that of Eqs. (2). All wave functions are understood to be antisymmetric under nucleon exchange. The exact matrix element for the two-particle stripping process can then be written as[4]

$$\mathfrak{M}_{fi}=\langle\Psi_f^-|\sum_{j=1}^{A}\sum_{k=1}^{N} V_{jk}|\Phi_i\rangle=\langle\Phi_f|\sum_{j=1}^{A+2}\sum_{k=1}^{N-2} V_{jk}|\Psi_i^+\rangle, \tag{4}$$

where $\Psi_f^-(\Psi_i^+)$ is an eigenfunction of energy E of the Hamiltonian H, with incoming (outgoing) wave boundary conditions.

In the approximation that the interaction of the incoming and outgoing systems with the relevant nuclei are represented by optical model potentials, the matrix element (to first order in the residual interaction) becomes[4]

$$\mathfrak{M}_{fi}\approx\langle X_f^-|\Delta V_i|X_i^+\rangle \approx\langle X_f^-|\sum_{j=1}^{N-2}\sum_{k=1}^{A} V_{jk}-\bar{V}_f+\sum_{j=1}^{N-2}(V_{j1}+V_{j2})|X_i^+\rangle, \tag{5}$$

where X_f^- and X_i^+ are eigenfunctions of energy E (with ingoing and outgoing wave boundary conditions,

[2] R. Serber, Phys. Rev. **72**, 1008 (1947).
[3] J. H. Manley, Phys. Rev. **130**, 1475 (1963).
[3a] *Note added in proof.* The forward peaking has now been observed for other targets as well; see J. H. Manley and W. E. Stein, Bull. Am. Phys. Soc. **8**, 611 (1963).
[4] M. Gell-Mann and M. L. Goldberger, Phys. Rev. **91**, 398 (1953).

respectively) of the Hamiltonians

$$\bar{H}_f=\sum_{k=1}^{A+N} T_k+\sum_{j=1}^{N-2}\sum_{k=j+1}^{N-2} V_{jk}+\sum_{j=1}^{A+2}\sum_{k=j+1}^{A+2} V_{jk}+\bar{V}_f, \quad (6a)$$

$$\bar{H}_i=\sum_{k=1}^{A+N} T_k+\sum_{j=1}^{N}\sum_{k=j+1}^{N} V_{jk}+\sum_{j=1}^{A}\sum_{k=j+1}^{A} V_{jk}+\bar{V}_i. \quad (6b)$$

Here $\bar{V}_f$ and $\bar{V}_i$ are, respectively, optical potentials of the interaction of the final $N-2$-body system with the nucleus $A+2$, and of the initial N-body system with the target A. The potential ΔV_i is the residual interaction, defined by

$$\Delta V_i=\sum_{j=1}^{A}\sum_{k=1}^{N} V_{jk}-\bar{V}_i.$$

The last form of Eq. (5) is more useful than the first one in the event that $\sum_{j=1}^{N-2}\sum_{k=1}^{A} V_{jk}-\bar{V}_f$ can be neglected. Arguments for this omission have been given in the past and are summarized by Tobocman.[5] With the neglect of this term, the distorted-wave Born-approximation matrix element becomes

$$\mathfrak{M}_{fi}=\langle X_f^-|\sum_{j=1}^{N-2}(V_{1j}+V_{2j})|X_i^+\rangle. \quad (7a)$$

In this work we shall restrict ourselves to an incident three-particle system (e.g., He^3, H^3), and for definiteness consider the (He^3,n) reaction.[6] It has the advantage of a single outgoing nucleon; furthermore, if the amplitude for spin-flip is small, there occur restrictive selection rules. Thus, if this amplitude is negligible, the two captured protons must be in a singlet spin state in the final nucleus, because this is their state in He^3. Since the two captured protons must also be in an isospin $T=1$ state, their relative spatial wave function must be an even one (i.e., orbital angular momentum even) and this further limits the nuclear states that can be reached.[7] However, all of the considerations developed below can easily be extended to other two-particle stripping reactions such as (α,d) processes. For the (He^3,n) reaction, Eq. (7a) reduces to

$$\mathfrak{M}_{fi}=\langle X_f^-|V_{n1}+V_{n2}|X_i^+\rangle, \quad (7b)$$

where 1 and 2 refer to the two protons and n to the neutron in He^3.

To carry the development further, it is necessary to introduce a specific nuclear model. We shall be most interested in nuclei near closed shells and will therefore take the spherical-shell model as the starting point in obtaining nuclear wave functions. For other targets, collective rotational effects can be of importance. To bring out and discuss the treatment of the spatial integrals in the matrix element, Eq. (7), we shall temporarily introduce several further simplifications:

(a) We assume L-S coupling to be valid. This is approximately satisfied for light p-shell nuclei.

(b) We take the two protons to be captured into pure shell-model states.

(c) We restrict ourselves to an initial state of the target that consists of a closed inert core (i.e., closed shell nucleus) of spin and parity 0^+ (also $T=0$). This core then plays no role in the matrix element, as it simply integrates out. The advantage of this assumption is that the spectroscopic factors are then trivial.

(d) We assume $A\rightarrow\infty$, or rather, neglect effects of order A^{-1}. The recoil effects due to finite A are simple kinematical factors which we shall include later on.

(e) Here and later we assume that V_{n1} and V_{n2} are spin- and isospin-independent central potentials.

With the above simplifying assumptions, the matrix element reduces to

$$\mathfrak{M}_\lambda^{(1)}=\sum_{m_1m_2\mu_1\mu_2}(l_1l_2m_1m_2|\lambda\nu)(\tfrac{1}{2}\,\tfrac{1}{2}\mu_1\mu_2|S\mu)\langle\zeta_{1/2}{}^{\mu_1}\zeta_{1/2}{}^{\mu_2}\zeta_{1/2}{}^{\mu_n}|\zeta_{1/2}{}^{\mu_{\mathrm{He}}}\rangle$$
$$\times\langle\chi_p^-(\mathbf{r}_n)\phi_{l_1}{}^{m_1}(\mathbf{r}_1)\phi_{l_2}{}^{m_2}(\mathbf{r}_2)|V_{n1}+V_{n2}|\chi_P^+(\mathbf{R}_{\mathrm{He}})\phi_{\mathrm{He}}[\mathbf{r}_1-\mathbf{r}_2,\ \mathbf{r}_n-\tfrac{1}{2}(\mathbf{r}_1+\mathbf{r}_2)]\rangle, \quad (8)$$

where $\mathbf{R}_{\mathrm{He}}=(\mathbf{r}_1+\mathbf{r}_2+\mathbf{r}_n)/3$, the ϕ's and χ's are spatial wave functions of the bound states and scattering states, respectively, and the ζ's are spin wave functions. The two proton final-state function should be antisymmetrized; however, the stripping interaction is symmetric and the initial state is antisymmetric under the exchange of 1 and 2. Thus, we need not explicitly antisymmetrize the final bound-state wave function. In Eq. (8) $(\cdots|\cdots)$ are Clebsch-Gordan coefficients and the subscript λ and the superscript (1) refer to the final nuclear state reached; λ stands for its angular momentum and energy and (1) for its isospin. If the internal relative state of the two protons in He^3 is taken to be purely $^1s_0$, then the spin sums in Eq. (8) are trivial and λ must be even since the isospin is 1. We thus find

$$\mathfrak{M}_\lambda{}^{(1)}=\delta_{\mu_n,\mu_{\mathrm{He}}}\mathfrak{M}_\lambda{}^{(1)}, \quad (9a)$$

with

$$\mathfrak{M}_\lambda{}^{(1)}=\sum_{m_1m_2}(l_1l_2m_1m_2|\lambda\nu)\langle\chi_p^-(\mathbf{r}_n)\phi_{l_1}{}^{m_1}(\mathbf{r}_1)\phi_{l_2}{}^{m_2}(\mathbf{r}_2)|V_{n1}+V_{n2}|\chi_P^+(\mathbf{R}_{\mathrm{He}})\phi_{\mathrm{He}}[\mathbf{r}_1-\mathbf{r}_2,\ \mathbf{r}_n-\tfrac{1}{2}(\mathbf{r}_1+\mathbf{r}_2)]\rangle. \quad (9b)$$

[5] W. Tobocman, *Theory of Direct Nuclear Reactions* (Oxford University Press, New York, 1961), Chap. III.
[6] The (H^3,p) reaction is symmetrical to that treated here, and differs from it chiefly due to Coulomb effects.
[7] See also H. C. Newns, Proc. Phys. Soc. (London) **76**, 489 (1960); N. K. Glendenning, Nucl. Phys. **29**, 109 (1962).

TABLE I. Values of the parameter γ determined by variational techniques and other means. The wave function v is given by $v=Nu^{-1/2}\exp[-(2)^{-1/2}\gamma\mu]$, with $u=(3r^2/2+2\xi^2)^{1/2}$, and N a normalization constant.

Reference	Method	Wave function	γ(F^{-1})
E. Guerjoy and J. Schwinger, Phys. Rev. **61**, 138 (1942).	Variation (including D wave)	Eq. (11)+D wave	0.33
J. Irving, Phil. Mag. **42**, 338 (1951).	Variation for H^3	v	$\sim$1
S. Suekane and W. Watari, Progr. Theoret. Phys. (Kyoto) **14**, 490 (1955).	Shell model	Eq. (11)	$\approx$0.39
Von W. Inthoff, Ann. Physik **3**, 220 (1959).	Shell model+variation ($\langle r_0^2\rangle$ is used to find γ)	Eq. (11)	0.27
H. J. Mang and W. Wild, Z. Physik **154**, 182 (1959).	Independent pair model	...	$\sim$0.5
W. Laskar, Ann. Phys. (N. Y.) **17**, 436 (1962).	Variation	Eq. (11)	0.39
Y. C. Tang, E. Schmid, and K. Wildermuth, Phys. Rev. **131**, 2631 (1963).	Cluster model, variation	Eq. (11)	0.384
H. Collard, R. Hofstadter, *et al.*, Phys. Rev. Letters **11**, 132 (1963).	Electron scattering	Eq. (11)	0.31
A. Goldberg and D. Krueger (private communication).	Analysis of electron scattering, including nucleon form factor	Eq. (11)+nucleon form factor	0.36
Weighted average of last 7 values			0.36

In terms of this matrix, the differential cross section is (0^+ target state)

$$\frac{d\sigma_\lambda}{d\Omega}=\frac{1}{4\pi^2}\frac{p}{P}3M_N{}^2\sum|\mathfrak{M}_\lambda{}^{(1)}|^2, \tag{10}$$

where M_N is the nucleon mass. Before evaluating the matrix $\mathfrak{M}_\lambda{}^{(1)}$, we shall discuss the spatial properties of the wave functions and interactions in Eq. (9b).

1. Internal Wave Function of He^3

For the space properties of He^3 we shall assume a completely symmetric s state of Gaussian form,

$$\begin{aligned}\phi_{\mathrm{He}}&=N_{\mathrm{He}}\exp\{-\tfrac{1}{2}\gamma^2[(\mathbf{r}_1-\mathbf{r}_2)^2+(\mathbf{r}_1-\mathbf{r}_n)^2+(\mathbf{r}_2-\mathbf{r}_n)^2]\}\\&=N_{\mathrm{He}}\exp[-\tfrac{1}{2}\gamma^2(\tfrac{3}{2}r^2+2\xi^2)],\end{aligned} \tag{11}$$

where N_{He} is a normalization constant,

$$N_{\mathrm{He}}=\gamma^3 3^{3/4}\pi^{-3/2},$$

and $\mathbf{r}=\mathbf{r}_1-\mathbf{r}_2$, $\boldsymbol{\xi}=\mathbf{r}_n-\frac{1}{2}(\mathbf{r}_1+\mathbf{r}_2)$. The value of the single parameter γ can be determined from two considerations: (a) electron-scattering experiments and (b) variational calculations for the ground-state energy. Several calculations of the latter type, or variants thereof, have been reported in the literature. We summarize their results in Table I. In this table we also include the value of γ deduced from the mean square radius $\langle r_0^2\rangle$, found from He^3 electron-scattering experiments.[8] We shall take $\gamma\approx0.36$ F^{-1}, which is the mean value of recent data (with double weight given to the electron-scattering data). The calculated differential cross section in the forward hemisphere will be shown to be relatively insensitive to γ, unless its value becomes $\lesssim$0.15. This corresponds to a r.m.s. radius of $\gtrsim$3.8 F, which is unreasonably large.

2. Stripping Interaction

For the potential $V_{n1}+V_{n2}$, we shall take a purely central Gaussian interaction:

$$V_{n1}+V_{n2}=V_0[e^{-\beta^2(\mathbf{r}_n-\mathbf{r}_1)^2}+e^{-\beta^2(\mathbf{r}_n-\mathbf{r}_2)^2}]. \tag{12a}$$

This form is simple to work with, as it allows many of the integrals to be evaluated analytically. Furthermore, for large β it can be made to simulate a δ-function interaction; if the strength and range are normalized so that the volume integrals are the same, we can write

$$\lim_{\beta\to\infty}V_0e^{-\beta^2r^2}\to\pi^{3/2}V_0\beta^{-3}\delta(\mathbf{r}), \tag{12b}$$

where β is to be taken finite on the right-hand side. In the development that follows, we shall retain a finite range β^{-1} but the limit of zero-range forces can be obtained by use of Eq. (12b).

3. Nuclear Wave Functions

For the radial parts of the nuclear wave functions of the captured protons, we shall, in most of this work, assume those of an infinite harmonic oscillator. For highly excited states these wave functions certainly differ in the asymptotic region from those of a particle in a finite well.[9] We shall discuss this effect below; for purposes of comparison with a finite potential, we shall carry out a simplified calculation with a potential of the Saxon type[10] for the bound protons. However, for

[8] H. Collard and R. Hofstadter, Phys. Rev. **131**, 416 (1963); H. Collard, R. Hofstadter, A. Johansson, R. Parks, M. Ryneveld, A. Walker, M. R. Yearian, R. B. Day, and R. T. Wagner, Phys. Rev. Letters **11**, 132 (1963).

[9] A further problem that can occur in the shell model generally is that spurious states may occur in which the center-of-mass of the nucleus is excited. See J. P. Elliott and T. H. R. Skyrme, Proc. Roy. Soc. (London) **A232**, 62 (1957). These states are not met in our work.

[10] See, for example, M. A. Melkanoff, J. S. Nodvik, D. S. Saxon, and R. D. Woods, Phys. Rev. **106**, 793 (1957).

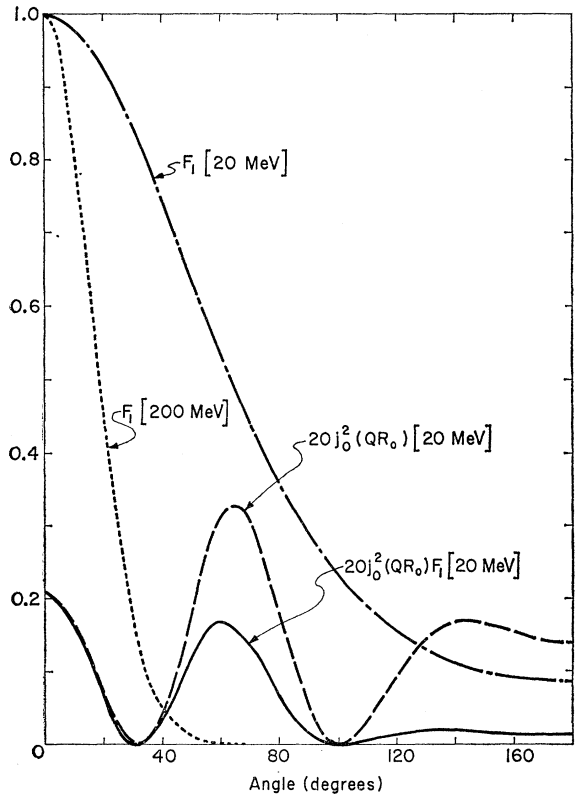

FIG. 1. Form factor $F_1(q^2)$ as a function of scattering angle for 20- and 200-MeV incident He^3 ions. $F_1=\exp[-q^2/2(\beta^2+\gamma^2)]$, and the curves are for $\beta=\gamma=0.36$ F^{-1} and $\mathbf{q}=\mathbf{P}/3-\mathbf{p}$ with $p=1/3P$. The effect of $F_1(q^2)$ on the plane-wave Born approximation at 20 MeV is also depicted for a spin zero-to-zero transition.

nuclear-bound states, we believe that the assumptions of an infinite well will influence mainly the magnitude of the cross section. Since there are many other parameters that affect this magnitude [e.g., the optical potential parameters (see Sec. III)], we feel that the assumption is justified with the present state of our knowledge. Furthermore, the finite well wave functions close to the nuclear surface can be reproduced by adjusting the natural frequency of the harmonic oscillator, as we shall show below.

The chief advantage of an infinite harmonic oscillator is that a two-particle state function separates into simple center-of-mass and relative-motion wave functions.[11] This separation is, of course, also possible for a finite well, but the expansion involves an infinite rather than a finite number of energy states. For two-particle bound states in a reasonably shaped finite well, one might expect that the expansion coefficients are large only for those states that are not zero for an infinite harmonic oscillator. In the latter case, the state function of two particles coupled to an angular momentum λ can be written as

$$\sum_{m_1m_2}(l_1l_2m_1m_2|\lambda\nu)\phi_{n_1l_1}{}^{m_1}(\mathbf{r}_1)\phi_{n_2l_2}{}^{m_2}(\mathbf{r}_2)$$
$$=\sum_{nlNLmM}H(nlNL,n_1l_1n_2l_2,\lambda)(lLmM|\lambda\nu)\times\phi_{NL}{}^{M}(\mathbf{R})\phi_{nl}{}^{m}(\mathbf{r}), \quad (13)$$

where $\mathbf{R}=\frac{1}{2}(\mathbf{r}_1+\mathbf{r}_2)$, $\mathbf{r}=(\mathbf{r}_1-\mathbf{r}_2)$, n_1, n_2, N, and n are principal quantum numbers, and H is a Talmi coefficient. These coefficients are independent of magnetic quantum numbers but depend on the angular momenta and principal quantum numbers. They have been tabulated in useful form by Brody and Moshinsky.[12]

B. Plane-Wave Born Approximations

For comparison with later developments, we shall first calculate the matrix element $\mathfrak{M}_\lambda{}^{(1)}$ in Born approximation. Then $\chi_p{}^-$ and $\chi_P{}^+$ are replaced by plane waves, and the matrix element can be evaluated analytically. This approximation has been amply discussed in the past.[1,7,13] However, it serves to bring out several interesting features not studied previously, especially those associated with the form and range of the stripping interaction and with the structure of He^3.

Substituting Eqs. (11), (12), and (13) into Eq. (9b), we obtain

$$\mathfrak{M}_\lambda{}^{(1)}=N_{\mathrm{He}}V_0\sum_{LNlnmM}H(nlNL,n_1l_1n_2l_2,\lambda)(lLmM|\lambda\nu)\langle\phi_{NL}{}^{M}(\mathbf{R})\phi_{nl}{}^{m}(\mathbf{r})\exp[i\mathbf{p}\cdot(\xi+\mathbf{R})]|\exp[-\beta^2(\xi+\tfrac{1}{2}\mathbf{r})^2]$$
$$+\exp[-\beta^2(\xi-\tfrac{1}{2}\mathbf{r})^2]|\exp[i\mathbf{P}\cdot(\mathbf{R}+\tfrac{1}{3}\xi)]\exp[-\tfrac{1}{2}\gamma^2(\tfrac{3}{2}r^2+2\xi^2)]\rangle. \quad (14)$$

The spatial integrations are carried out below with and without further assumptions.

1. Simplified Interaction

In the spirit of the optical model we can approximate the interaction of the neutron with the two protons by that with their center-of-mass only,

$$V_0\{\exp[-\beta^2(\xi+\tfrac{1}{2}\mathbf{r})^2]+\exp[-\beta^2(\xi-\tfrac{1}{2}\mathbf{r})^2]\}\approx 2V_0'\exp(-\beta^2\xi^2).$$

In this case, the matrix element separates into three factors

$$\mathfrak{M}_\lambda{}^{(1)}=2V_0'N_{\mathrm{He}}\sum_{LNlnmM}H(nlNL,n_1l_1n_2l_2,\lambda)\times(lLmM|\lambda\nu)\mathfrak{M}_L\mathfrak{M}_{\beta\gamma}\mathfrak{M}_l, \quad (15)$$

[11] I. Talmi, Helv. Phys. Acta **25**, 185 (1952).

[12] T. A. Brody and M. Moshinsky, *Tables of Transformation Brackets* (Institute of Physics, University of Mexico, 1960). This reference uses $\mathbf{r}=(2)^{-1/2}(\mathbf{r}_1-\mathbf{r}_2)$ and $\mathbf{R}=(2)^{-1/2}(\mathbf{r}_1+\mathbf{r}_2)$ whereas we shall use $\frac{1}{2}\alpha^2$ and $2\alpha^2$ for the relative and center-of-mass harmonic oscillator parameters, respectively. The single-particle value of α^2 is related to the harmonic oscillator frequency ω by $\alpha^2=M_N\omega$, where M_N is the nucleon mass.

[13] M. El Nadi, Proc. Phys. Soc. (London) **A70**, 62 (1957).

with

$$\mathfrak{M}_L \equiv \langle \phi_{NL}{}^M(\mathbf{R}) e^{i\mathbf{p}\cdot\mathbf{R}} | e^{i\mathbf{P}\cdot\mathbf{R}} \rangle,$$
$$\mathfrak{M}_{\beta\gamma} \equiv \langle \exp(i\mathbf{p}\cdot\boldsymbol{\xi}) | e^{-\beta^2\xi^2} | \exp(\tfrac{1}{3}i\mathbf{P}\cdot\boldsymbol{\xi}) \exp(-\gamma^2\xi^2) \rangle,$$
$$\mathfrak{M}_l \equiv \langle \phi_{nl}{}^m(\mathbf{r}) | e^{-\frac{1}{4}\gamma^2 r^2} \rangle.$$

In the subsections below, we shall briefly discuss the effects on the cross section of each integral or submatrix of Eq. (15).

(*a*) $\mathfrak{M}_L$. If $\phi_{NL}{}^M(\mathbf{R})$ is concentrated close to the nuclear surface, or if the first integral's main contribution is assumed to occur close to $R=R_0$ (see Sec. IV), then we obtain the usual factor[14]

$$\langle \phi_{NL}{}^M(\mathbf{R}) e^{i\mathbf{p}\cdot\mathbf{R}} | e^{i\mathbf{P}\cdot\mathbf{R}} \rangle \approx \delta_{M,0}[4\pi(2L+1)]^{1/2} \times i^L (R_0^2/\alpha') \mathcal{R}_{N\lambda}(R_0) j_L(QR_0). \quad (16)$$

In Eq. (16), α' is related to the binding energy B of $\phi_{NL}{}^M$ by $\alpha'^2 = 4M_N B$, $\mathcal{R}_{NL}$ is the radial part of $\phi_{NL}{}^M$, and $\mathbf{Q} \equiv \mathbf{P} - \mathbf{p}$ is taken as the axis of quantization. Other "more realistic" approximations for evaluating the integral in Eq. (16) are summarized by Tobocman.[14] The square of the Bessel function in Eq. (16) characterizes the angular distribution for the process being considered.

(*b*) $\mathfrak{M}_{\beta\gamma}$. The second overlap in Eq. (15) contributes[15]

$$|\mathfrak{M}_{\beta\gamma}|^2 = [\pi/(\gamma^2+\beta^2)]^3 F_1(q^2),$$
$$F_1(q^2) = e^{-q^2/2(\beta^2+\gamma^2)} \quad (17)$$

to the cross section, if $\mathbf{q} = \mathbf{P}/3 - \mathbf{p}$. This "form factor," due in part to the structure of He^3, has been discussed by El Nadi[13] and Newns.[7] A similar form factor is present in the Born-approximation treatment of deuteron-stripping reactions (due to the internal structure of H^2); there has been considerable discussion[16] whether it should be included in extended treatments (e.g., optical-model description) and whether the fit to experiment indicates its presence. It occurs because the structure of the incident system may limit available momenta. However, it should be noted that the form factor is determined not only by this structure, but also by the range (and, as we shall see, the nature) of the stripping interaction. Since He^3 is a fairly closely packed nucleus, the structure of which is partially determined by the range of the internucleon force, we expect β and γ to be comparable. This is different than deuterium, for which the radius is large compared to the range of the internucleon potential. For very short-range forces, or more precisely, for a zero-range force, we can normalize so that the binding energy of He^3 is reproduced[17] [rather than by means of Eq. (11b)],

$$\lim_{\beta\to\infty} V_0 e^{-(\gamma^2+\beta^2)\xi^2} = C_0 \delta(\boldsymbol{\xi}).$$

The form factor is then simply a constant. For a finite range force and at medium energies the form factor, Eq. (17), gives rise to a modulation envelope of the more rapidly varying angular distribution, determined by $j_L{}^2(QR_0)$ [see Eq. (16)].

(*c*) $\mathfrak{M}_l$. This last submatrix is a simple overlap integral because we chose the stripping potential to depend only on ξ. The integral is zero unless $l=m=0$. Furthermore, its main contribution will occur for $n=1$, since only then is $\phi_{nl}{}^m$ nodeless. In fact, if the single-particle oscillator parameter $\alpha = (3)^{1/2}\gamma$, then only the overlap with the $n=1$ state is nonvanishing; if $\phi_{nl}{}^m$ is $\phi_{10}{}^0$, the matrix element $\mathfrak{M}_l$ becomes

$$\mathfrak{M}_l = [(2\pi)^{1/2} 2\alpha^{-1}(1+3\gamma^2/\alpha^2)^{-1}]^{3/2} \delta_{l,0}, \quad (18a)$$

where α is the single-particle oscillator parameter.[12]

The above considerations are not greatly affected by short-range nuclear correlations, since these are of primary importance in relative s states. In particular, we may approximate the effects of these correlations by multiplying the simple shell-model wave function $\phi_{10}{}^0(r)$ by a correlation factor, $f(r)$,

$$f(r) = 0 \quad \text{for} \quad r < r_c \approx 0.4 \text{ F}$$
$$= 1 - e^{-\delta[(r/r_c)^2-1]} \quad \text{for} \quad r \geq r_c, \ \delta \approx 1,$$

as suggested by Dabrowski[18] and others. The overlap integral then becomes

$$\mathfrak{M}_l = \left(\frac{\pi\alpha^2}{2}\right)^{3/4} \left\{ \frac{1}{s^3}\left[1 + \frac{2sr_c}{(\pi)^{1/2}} e^{-s^2 r_c^2} - \operatorname{erf}(sr_c) \right] + \frac{e}{s'^3}\left[1 + \frac{2s'r_c}{(\pi)^{1/2}} e^{-s'^2 r_c^2} + \operatorname{erf}(s'r_c) \right] \right\}, \quad (18b)$$

where $s^2 = \frac{1}{4}(3\gamma^2+\alpha^2)$, $s'^2 = s^2 + r_c^{-2}$, and erf is the error function.[19] Thus, the numerical value of $\mathfrak{M}_l$ is slightly altered by these effects, but we still expect the nodeless $\phi_{10}{}^0$ to give the dominant contribution.

If, instead of treating the two protons as being bound in single-particle states of an infinite harmonic oscillator, we take them to be a point diproton captured into states of a finite Saxon well, then $\mathfrak{M}_\lambda{}^{(1)}$ becomes

$$\mathfrak{M}_\lambda{}^{(1)} = (16/\gamma^3)(\pi/3)^{3/2} V_0' N_{\mathrm{He}} \sum_{m_1 m_2} (l_1 l_2 m_1 m_2 | \lambda\nu) \mathfrak{M}_{\beta\gamma} \times \langle \phi_{n_1 l_1}{}^{m_1}(\mathbf{R}) \phi_{n_2 l_2}{}^{m_2}(\mathbf{R}) e^{i\mathbf{p}\cdot\mathbf{R}} | e^{i\mathbf{P}\cdot\mathbf{R}} \rangle \delta_{n_1,n_2} \delta_{l_1,l_2},$$

with $\mathfrak{M}_{\beta\gamma}$ defined as in Eq. (15).

[14] See W. Tobocman, Ref. 5, Chap. II.
[15] G. N. Watson, *Theory of Bessel Functions* (Cambridge University Press, Cambridge, 1958), p. 394.
[16] See, for example, D. A. Bromley, J. A. Kuehner, and E. Almquist in *Proceedings of the International Conference on Nuclear Structure, 1960*, edited by D. A. Bromley and E. W. Vogt (North-Holland Publishing Company, Amsterdam, 1960), p. 349; R. Middleton and S. Hinds, Nucl. Phys. **34**, 404 (1962).
[17] W. Tobocman, Ref. 5, p. 35.
[18] J. Drabowski, Proc. Phys. Soc. (London) **71**, 658 (1958); C. M. Shklyarevsky, Zh. Eksperim. i Teor. Fiz. **39**, 1031 (1961) [English transl: Soviet Phys.—JETP **12**, 717 (1961)].
[19] E. Jahnke and F. Emde, *Tables of Functions* (Dover Publications, New York, 1945), 4th ed., p. 23.

(*d*) *Cross section.* By combining Eqs. (15), (16), (17), and (18a), we obtain for the complete matrix element ($n=1$, $l=0$, $L=\lambda$)

$$\mathfrak{M}_\lambda^{(1)}=32\pi^2(\tfrac{1}{2}\pi)^{3/4}i^\lambda(2\lambda+1)^{1/2}\delta_{\nu,0}V_0'N_{\mathrm{He}}\mathfrak{R}_{N\lambda}(R_0)R_0^2 \times H(nlNL,n_1l_1n_2l_2,\lambda) \times\alpha^{3/2}\alpha'^{-1}[(\gamma^2+\beta^2)(\alpha^2+3\gamma^2)]^{-3/2} \times j_\lambda(QR_0)e^{-q^2/4(\beta^2+\gamma^2)}, \quad (19)$$

with $N=n_1+n_2+\frac{1}{2}(l_1+l_2-\lambda)-1$. The differential cross section thus becomes [see Eq. (10)]

$$d\sigma_\lambda/d\Omega=C_BR_0^2j_\lambda^2(QR_0)F_1(q^2), \quad (20)$$

with

$$C_B=576(6\pi)^{1/2}(2\lambda+1)\frac{p}{P}(M_NR_0)^2\frac{V_0'^2}{\alpha'^2}\frac{\mathfrak{R}_{N\lambda}^2(R_0)}{\gamma^3} \times H^2(10N\lambda,n_1l_1n_2l_2,\lambda)\left[\frac{(\alpha/\gamma)}{(1+\beta^2/\gamma^2)(1+3\gamma^2/\alpha^2)}\right]^3.$$

At medium energies (10–50 MeV), the angular distribution is primarily determined by the oscillatory factor $j_\lambda^2(QR_0)$ with λ equal to the angular momentum of the final state. However, for higher energy incident projectiles, where several nuclear states may be excited, or for experiments which do not resolve several final states, these oscillations may tend to wash out; for example, if QR_0 is sufficiently large that an asymptotic expansion is valid, then $\sum_\lambda j_\lambda^2(QR_0)\approx$ constant.[20] The form factor $F_1(q^2)$ may then give rise to the dominant angular distribution. This is the limit described by Serber stripping,[2] with an angular distribution determined primarily by the internal structure of He^3. The effect of the modulation is shown in Fig. 1, for 20-MeV incident He^3 ions (for $\lambda=0$) as well as for 200-MeV He^3 ions. For illustration, we have taken the magnitude of the neutron momentum p to be $|\mathbf{p}|=|\mathbf{P}|/3$ and a nuclear radius of 5 F. We note that at 20 MeV the half-width of the modulation envelope is of the order of 65° if $\beta=\gamma=0.36$ F^{-1}. For a shorter (more reasonable) range β^{-1} of the interaction, the effect of the modulation is even smaller. If β and γ are taken to be equal, then they must be as small as 0.13 F^{-1} in order for the modulation envelope to be 1/10th of its forward value when the first minimum of the zeroth-order Bessel function is reached. This is not physically reasonable. On the other hand, for 200-MeV He^3 ions, the form factor (with $\beta=\gamma=0.36$ F^{-1}) reaches 1/10th of its forward value at about 35°. If the measurements at this energy include excitation of several states (of both odd and even parity), the form factor is expected to determine the angular variation.

[20] However, if primarily collective states, or more generally only even (odd) spin states, are excited, then the sum involves only even (odd) integers, and the above conclusion is not valid. Instead, the Blair phase rule [see J. S. Blair, *Proceedings of the International Conference on Nuclear Structure, 1960*, edited by D. A. Bromley and E. W. Vogt (The University of Toronto Press, Toronto, 1960), p. 824] tells us that for even spin states, for example, the angular distribution is $\propto j_0^2(QR_0)$.

2. Full Interaction

If the approximation is not made that the neutron interacts with the center-of-mass of the two protons, then it is simpler to consider separately (a) a zero-range potential and (b) a finite-range interaction, even though the former can be obtained from the latter by letting $\beta\to\infty$ in the exponent [see Eq. (12b)].

(*a*) *Zero-range interaction.* If the range of the stripping force is taken to be small compared to the radius of He^3, then

$$V_{1n}+V_{2n}=v_0[\delta(\boldsymbol{\xi}+\tfrac{1}{2}\mathbf{r})+\delta(\boldsymbol{\xi}-\tfrac{1}{2}\mathbf{r})]. \quad (21)$$

The matrix element $\mathfrak{M}_\lambda^{(1)}$ becomes

$$\mathfrak{M}_\lambda^{(1)}=2v_0N_{\mathrm{He}}\sum_{LN\,lnmM}(lLmM\,|\,\lambda\nu)H(nlNL,n_1l_1n_2l_2,\lambda) \times\langle\phi_{NL}^M(\mathbf{R})e^{i\mathbf{p}\cdot\mathbf{R}}\,|\,e^{i\mathbf{P}\cdot\mathbf{R}}\rangle \times\langle\phi_{nl}^m(\mathbf{r})e^{i(1/2)\mathbf{p}\cdot\mathbf{r}}\,|\,e^{i(1/6)\mathbf{P}\cdot\mathbf{r}}e^{-\gamma^2r^2}\rangle. \quad (22)$$

The dominant change from approximation (1) occurs in the matrix element which involves the structure of He^3. If the major contribution in the second matrix of (22) comes from values of $\frac{1}{2}qr$ that are small compared to unity, then the overlap integral will be small if $l\neq0$. We thus expect the $1s$ contribution to be most important, and neglect all other relative motion diproton states. At medium incident energies the rapid variation of the angular distribution is then the same as that given by Eq. (16) (with the same approximation) but the modulation envelope is replaced by

$$|\langle\phi_{nl}^m(\mathbf{r})\,|\,e^{-\gamma^2r^2}e^{i\frac{1}{2}\mathbf{q}\cdot\mathbf{r}}\rangle|^2=(8\pi)^{3/2}\frac{\alpha^3}{(\alpha^2+4\gamma^2)^3}F_2(q^2), \quad (23)$$

$$F_2(q^2)=e^{-q^2/2(\alpha^2+4\gamma^2)}.$$

The angular dependence of the cross section is thus

$$d\sigma/d\Omega\propto j_\lambda^2(QR_0)F_2(q^2). \quad (24)$$

The modulation envelopes given by Eq. (23) and Eq. (17) are compared in Fig. 2 for incident 20-MeV He^3 ions, with $\alpha/(3)^{1/2}=\gamma=\beta=0.36$ F^{-1}. The half-width of Eq. (23) is 160° as compared to 65° obtained with approximation (1). It is thus negligible in the forward hemisphere. We have used this example to illustrate the model-sensitivity of the modulation envelope.

(*b*) *Finite-range interaction.* Finally, we shall treat the case of the full interaction (12a) in Born approximation. The matrix element is then given by Eq. (14). We shall continue to assume that only relative s states of the two protons need be taken into consideration, but will not restrict ourselves to the $1s$ state. In that case the matrix element reduces to

$$\mathfrak{M}_\lambda^{(1)}=2N_{\mathrm{He}}V_0\sum_M H(n0NL,n_1l_1n_2l_2,\lambda) \times\delta_{M,\nu}\delta_{L,\lambda}\mathfrak{M}_L\mathfrak{M}_{l'}, \quad (25)$$

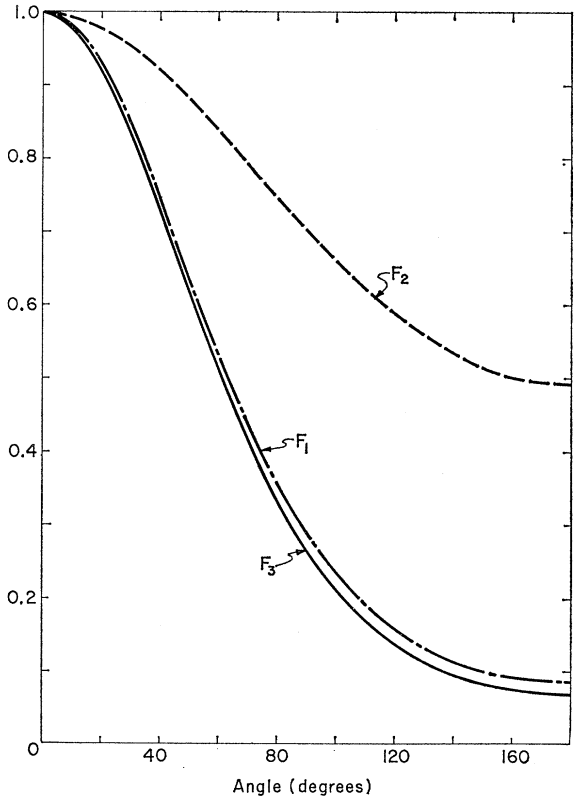

FIG. 2. Comparison of form factors F_1 [Eq. (17)], F_2 [Eq. (23)] and F_3 [Eq. (28)] as a function of scattering angle. F_1 is the form factor for a simplified Gaussian stripping interaction, F_2 is that for a point interaction, and F_3 corresponds to the full finite range Gaussian interaction. The curves are for 20-MeV incident He^3 ions, and $\beta=\gamma=\alpha/(3)^{1/2}=0.36$ F^{-1}.

with

$$\mathfrak{M}_L=\langle\phi_{NL}{}^M(\mathbf{R})\,|\exp(i\mathbf{Q}\cdot\mathbf{R})\rangle,$$

$$\mathfrak{M}_l'=\langle\phi_{n0}{}^0(\mathbf{r})\times|\tfrac{1}{2}\{\exp[-\beta^2(\xi+\tfrac{1}{2}\mathbf{r})^2]+\exp[-\beta^2(\xi-\tfrac{1}{2}\mathbf{r})^2]\}|\times\exp(i\mathbf{q}\cdot\xi)\exp[-\gamma^2(\tfrac{3}{4}r^2+\xi^2)]\rangle.$$

The matrix $\mathfrak{M}_L$ (evaluated at the nuclear surface) is again that of Eq. (16), but the second matrix $\mathfrak{M}_l'$ no longer separates into a product of two submatrices. The integrals can be carried out, nevertheless. After integrating over $\mathbf{r}$, we obtain

$$\mathfrak{M}_l'=\pi^{3/2}\sum_{j=0}^{n-1}(-1)^jC_{nj}\left(\frac{\alpha^2}{2}\right)^j\frac{\partial^j}{(\partial f^2)^j}\frac{1}{f^3}\times\int\exp(-g^2\xi^2)\exp(i\mathbf{q}\cdot\xi)d^3\xi, \quad (26)$$

where $f^2=\frac{1}{4}(\beta^2+3\gamma^2+\alpha^2)$, $g^2=\gamma^2+\beta^2-\beta^4/4f^2$, and $\phi_{n0}{}^0$ has been written as

$$\phi_{n0}{}^0=\sum_{j=0}^{n-1}C_{nj}\left(\frac{\alpha^2}{2}\right)^j r^{2j}e^{-(\alpha^2/4)r^2}.$$

The coefficients C_{nj} are given by an expansion of Laguerre polynomials.[21] The integration over ξ is now readily carried out, and we find

$$\mathfrak{M}_l'=\pi^3\sum_{j=0}^{n-1}(-1)^jC_{nj}\left(\frac{\alpha^2}{2}\right)^j\frac{\partial^j}{(\partial f^2)^j}\frac{1}{f^3}\frac{1}{g^3}e^{-q^2/4g^2}. \quad (27)$$

With the use of Eq. (16), the differential cross section becomes

$$d\sigma/d\Omega=C_cR_0{}^2j_\lambda{}^2(QR_0)F_3(q^2), \quad (28)$$

with

$$F_3(q^2)=e^{-q^2/2g^2},$$

and

$$C_c=3^{3/2}12\pi^2(2\lambda+1)\left(\frac{V_0}{\alpha'}\right)^2\frac{p}{P}(M_NR_0)^2\times e^{q^2/2g^2}\left|\sum_{Nnj}\frac{\mathcal{R}_{N\lambda}(R_0)}{\gamma^{3/2}}H(n0N\lambda,n_1l_1n_2l_2,\lambda)\times(-1)^j\frac{C_{nj}}{\gamma^{3/2}}\left(\frac{\alpha^2}{2}\right)^j\frac{\partial^j}{(\partial f^2)^j}\frac{\gamma^6}{f^3g^3}e^{-q^2/4g^2}\right|^2.$$

As shown before, the angular distribution is determined chiefly by $j_\lambda{}^2(QR_0)$ at medium energies. For 20-MeV He^3 ions, if we take $\beta^2=\gamma^2=\alpha^2/3$, and keep only the $n=1$ term in Eq. (28), the modulation envelope differs very little from that of Eq. (20) (the magnitude of the exponent is increased by 7% from its value in that section), since $\beta^2/4f^2\ll1$ (see Fig. 2).

C. Optical Model (Distorted-Wave Born Approximation)

We have gone into a fair amount of detail in the plane-wave Born approximation in Sec. II B because many considerations discussed there also apply in a distorted-wave description of the (He^3,n) reaction.

In the center-of-mass system, the optical-model wave function for the initial and final state are [see Eq. (5)]

$$X_i{}^+=\chi_K{}^+(\mathbf{R}+\tfrac{1}{3}\xi)\phi_{J_i,t_i}{}^{M_i,\nu_i}(1,\cdots,A)\phi_{\mathrm{He}}(\xi,r)\times[\zeta_{1/2}{}^{\nu_{\mathrm{He}}}\rho_{1/2}{}^{1/2}(\mathrm{He})], \quad (29)$$

$$X_f{}^-=\chi_k{}^-\left(\xi+\frac{A}{A+2}\mathbf{R}\right)\zeta_{1/2}{}^{\nu_n}\rho_{1/2}{}^{-1/2}(n)\times\phi_{J_f,t_f}{}^{M_f,\nu_f}(1,\cdots,A+2), \quad (30)$$

where the initial relative momentum $\mathbf{K}$ is related to the laboratory momentum $\mathbf{P}$ by $\mathbf{K}=\mathbf{P}[A/(A+3)]$ and the final relative momentum $\mathbf{k}$ to its laboratory counterpart by $\mathbf{k}=[(A+2)/(A+3)]\mathbf{p}$. The antisymmetric wave functions $\phi_{J_i,t_i}{}^{M_i,\nu_i}$ and $\phi_{J_f,t_f}{}^{M_f,\mu_f}$ are the (space-spin-isospin) wave functions for the initial and final nuclear

[21] See, for example, A. de Shalit and I. Talmi, *Nuclear Shell Theory* (Academic Press Inc., New York, 1963), pp. 39–41.

states, respectively, the subscripts and superscripts referring to the angular momentum and isospin of the respective states.[22] The functions ρ are isospin wave functions, and $[\rho_{1/2}{}^{1/2}(\mathrm{He})\zeta_{1/2}{}^{\nu_{\mathrm{He}}}]$ is the totally antisymmetric spin-isospin wave function for He^3. We shall immediately generalize our earlier discussion to j-j coupling, but will continue to use the shell model (with configuration mixing allowed). The final-state nuclear wave function can then be written as

$$\phi_{J_f}{}^{M_f}(1,\cdots,A+2)=\sum_{JMJ_i'M_i't_i'\nu_i'j_1j_2}B_{t_i't_f}(j_1j_2J,J_i'J_f)\times(J_i'JM_i'M\,|\,J_fM_f)(t_i'1\nu_i'1\,|\,t_f\nu_f)\phi_{J_i't_i'}{}^{M_i'\nu_i'}(1,\cdots,A)\phi_J{}^M(\mathbf{R}+\tfrac{1}{2}\mathbf{r},\mathbf{R}-\tfrac{1}{2}\mathbf{r})\rho_1{}^1(1,2)\,, \quad (31)$$

where j_i refers to the total angular momentum of each captured proton (principal quantum numbers are omitted for brevity), and B is related to the usual spectroscopic factor.[23] The two-proton final-state function ϕ_J need not be antisymmetrized [see the discussion following Eq. (8)].[24] Thus, we write

$$\begin{aligned}\phi_J(\mathbf{r}_1,\mathbf{r}_2)&=\sum_{m_1m_2}(j_1j_2m_1m_2\,|\,JM)\phi_{j_1}{}^{m_1}(\mathbf{r}_1)\phi_{j_2}{}^{m_2}(\mathbf{r}_2)\\&=\sum_{\lambda S\nu\nu'}T^\dagger(j_1j_2J,LSJ)(\lambda S\nu\nu'\,|\,JM)\phi_\lambda{}^\nu(\mathbf{r}_1,\mathbf{r}_2)\zeta_S{}^{\nu'}(1,2)\\&=\sum_{\lambda S\nu\nu' nlNLM'm}T^\dagger(j_1j_2J,LSJ)(\lambda S\nu\nu'\,|\,JM)(lLmM'\,|\,\lambda\nu)H(nlNL,n_1l_1n_2l_2,\lambda)\phi_L{}^{M'}(\mathbf{R})\phi_l{}^m(\mathbf{r})\zeta_S{}^{\nu'}(1,2)\,, \quad (32)\end{aligned}$$

where the last form is obtained by transforming to L-S coupling,[25] and then to center-of-mass and relative coordinates.[11,12] The cross section for the stripping process thus becomes [compare to Eq. (10)]

$$\begin{aligned}\frac{d\sigma}{d\Omega}=&\frac{1}{4\pi^2}\frac{\mu_i\mu_f}{K}\frac{k}{2J_i+1}\tfrac{1}{2}\sum_{M_fM_i\nu_n\nu_{\mathrm{He}}}\Big|\sum B_{t_it_f}(j_1j_2J,J_iJ_f)\\&\times(J_iJM_iM\,|\,J_fM_f)(t_i1\nu_i1\,|\,t_f\nu_f)T^\dagger(j_1j_2J,LSJ)(\lambda S\nu\mu\,|\,JM)H(nlNL,n_1l_1n_2l_2,\lambda)(lLmM'\,|\,\lambda\nu)\\&\times\Big\langle\phi_L{}^{M'}(\mathbf{R})\phi_l{}^m(\mathbf{r})\zeta_S{}^{\nu'}(1,2)\chi_k{}^-\Big(\xi+\frac{A}{A+2}\mathbf{R}\Big)\zeta_{1/2}{}^{\nu_n}(n)\,\Big|\,V_{n1}+V_{n2}\,\Big|\,\chi_K{}^+(\mathbf{R}+\tfrac{1}{3}\xi)\zeta_{1/2}{}^{\nu_{\mathrm{He}}}(1,2,n)\phi_{\mathrm{He}}(\xi,\mathbf{r})\Big\rangle\Big|^2\,, \quad (33)\end{aligned}$$

where μ_i and μ_f are the reduced masses of the initial and final system, respectively. In Eq. (33), and in the evaluation thereof, the following assumptions are made: (a) no spin-orbit coupling occurs in the optical potentials, (b) the stripping interaction is spin- (and isospin-) independent, (c) the two protons are coupled to spin zero in He^3, and (d) the initial nucleus acts as an inert core; that is except for antisymmetrization effects, all excited states as well as the ground state of the final nucleus are assumed to arise from the two added protons.[26] In addition, we shall make the assumption (e) that, in the final nuclear state, the two protons have almost no overlap with the initial He^3 internal wave function unless $\phi_{nl}{}^m(\mathbf{r})$ is an s state. This last assumption has been discussed in Sec. IIB; we shall not yet restrict ourselves to the $1s$ state. It should be noted that all of these assumptions can be relaxed, but at the expense of additional complexity. We believe, furthermore, that the premises listed above can be justified on physical grounds. The neglect of spin-orbit coupling, for example, is not expected to affect the angular distribution in the forward hemisphere, which is the region of primary interest to us. After summing over final and initial magnetic quantum numbers, the cross section reduces to

$$\frac{d\sigma}{d\Omega}=\frac{1}{4\pi^2}\frac{\mu_i\mu_f}{K}\frac{k}{2J_i+1}\frac{2J_f+1}{}(t_i1\nu_i1\,|\,t_f\nu_f)^2\sum_{JM}\frac{1}{(2J+1)}\Big|\sum_{j_1j_2}B_{t_it_f}(j_1j_2J\,;J_iJ_f)\times T^\dagger(j_1j_2J\,;J0J)H(n0NJ,n_1l_1n_2l_2,J)\mathfrak{M}_J\Big|^2\,, \quad (34)$$

[22] For heavy target nuclei the isospin labels should be omitted. We include them here for completeness.
[23] See S. Yoshida, Ref. 1; also M. H. Macfarlane and J. B. French, Rev. Mod. Phys. **32**, 567 (1960).
[24] However, when summing over j_1 and j_2, one must remember the normalization factor $[2/(1+\delta_{j_1,j_2})]^{1/2}$.
[25] M. E. Rose, *Elementary Theory of Angular Momentum* (John Wiley & Sons, Inc., New York, 1957), Chap. XI.
[26] Some experimental evidence for the validity of this approximation in two-particle stripping is given by J. Cerny, B. G. Harvey, and R. H. Pehl, Nucl. Phys. **29**, 120 (1962).

with

$$\mathfrak{M}_J=\left\langle \chi_k^-\left(\xi+\frac{A}{A+2}\mathbf{R}\right)\phi_{NJ}{}^M(\mathbf{R})\phi_{n0}{}^0(\mathbf{r})\,|\,V_{n1}+V_{n2}\,|\,\chi_K^+(\mathbf{R}+\tfrac{1}{3}\xi)\phi_{\mathrm{He}}(\xi,\mathbf{r})\right\rangle.$$

After substituting Eqs. (11) and (12a), the $\mathbf{r}$ integration can be carried out as for Eq. (25), and we obtain

$$\mathfrak{M}_J=2V_0\pi^{3/2}N_{\mathrm{He}}\sum_{j=0}^{n-1}(-1)^jC_{nj}\left(\frac{\alpha^2}{2}\right)^j\frac{\partial^j}{(\partial f^2)^j}\frac{1}{f^3}\int e^{-g^2\xi^2}\chi_k^{-*}\left(\xi+\frac{A}{A+2}\mathbf{R}\right)\phi_{NJ}{}^M(\mathbf{R})\chi_K^+(\mathbf{R}+\tfrac{1}{3}\xi)d^3\xi d^3R. \quad (35)$$

The integration over the relative neutron coordinate ξ cannot be carried out in closed form in the distorted-wave approximation. A reasonable approximation for the evaluation of the integral appears to be achieved if we change variables to ξ and $\mathbf{X}=R+\xi/3$ in Eq. (35) and then only neglect the ξ dependence of χ_k^- [i.e., not that of $\phi_{NJ}{}^M(\mathbf{X}-\xi/3)$]. The trouble is that this is reasonable only if both the expectation value of $|\xi|$ is much smaller than that of $|\mathbf{X}|$ and $k\ll g$.[27] Whereas the former justification obtains, since the radius of He^3 is small compared to that of most target nuclei, it is difficult to justify $k\ll g$. In fact, if $\beta=\gamma$ and for 10–15 MeV neutrons, $k\approx g$.

If the phasing remains approximately the same in χ_k^- and χ_K^+ as for the Born approximation, then one might think of writing

$$\begin{aligned}\chi_k^-\left(\frac{A}{A+2}\mathbf{R}+\xi\right)&\approx\chi_k^-\left(\frac{A}{A+2}\mathbf{R}\right)\exp(i\mathbf{k}\cdot\xi),\\ \chi_K^+\left(\frac{A}{A+2}\mathbf{R}+\tfrac{1}{3}\xi\right)&\approx\chi_K^+\left(\frac{A}{A+2}\mathbf{R}\right)\exp(i\tfrac{1}{3}\mathbf{K}\cdot\xi).\end{aligned} \quad (36)$$

Although we considered the use of Eq. (36), we could not find any reason for such a separation, and we shall not employ it below. However, we would like to point out that with Eq. (36) one obtains the form factor $\exp(-q^2/2g^2)$, [see Eq. (28)]. As we saw earlier, this factor is not important in the forward hemisphere and the "$2g^2$" in the exponent depends on the model of the stripping interaction.

A better approximation for evaluating $\mathfrak{M}_J$ than the change of variable discussed earlier appears to be the neglect of the ξ dependence of both χ_k^- and χ_K^+. The reason that we feel this is a better approximation is that in Born approximation phasing, the criterion that k be much less than g is replaced by $q/g=|\mathbf{K}/3-\mathbf{k}|/g\ll1$, and the latter is valid at medium energies, as we argued earlier. With the described optical-model approximation, no form factor occurs in the cross section; we obtain for $\mathfrak{M}_J$

$$\mathfrak{M}_J=2V_0N_{\mathrm{He}}\pi^3\sum_{j=0}^{n-1}(-1)^jC_{nj}\times\left(\frac{\alpha^2}{2}\right)^j\frac{\partial^j}{(\partial f^2)^j}\frac{1}{f^3}\frac{1}{g^3}\mathfrak{M}_J', \quad (37a)$$

with

$$\mathfrak{M}_J'=\int\chi_k^{-*}\left(\frac{A}{A+2}\mathbf{R}\right)\phi_{NJ}{}^{M*}(\mathbf{R})\chi_K^+(\mathbf{R})d^3R. \quad (37b)$$

By comparison, if we make the approximation suggested first (of changing variables to $\mathbf{X}$ and ξ) we obtain

$$\mathfrak{M}_J'=27\int\chi_k^{-*}\left(\frac{A}{A+2}\mathbf{X}\right)\chi_K^+(\mathbf{X})e^{-9g^2X^2}\times\sum_{l=0}^{N-1}C_{Nl}\frac{\partial^l}{(\partial h^2)^l}\frac{(9g^2X)^J}{h^{2J+3}}e^{81g^4X^2/h^2}d^3X, \quad (38)$$

with $h^2=9g^2+\alpha^2$. Since $9g^2\gg\alpha^2$, we can expand to obtain in leading order, the same expression as Eq. (37b) with $\mathbf{R}$ replaced by $\mathbf{X}$. To the next order, for $N=1$, for example, we find the same expression as (38), except that the integrand is multiplied by $\exp[(\alpha^2X^2)(\alpha^2/9g^2)]$. Thus, to leading order, the same result is found with either approximation. The correction term for $N=1$ intimates that perhaps a smaller value of α should be used than that suggested by pure shell-model considerations. This is a further reason to keep the harmonic oscillator energy spacing variable.

The evaluation of the matrix element is now complete except for an integration over $\mathbf{R}$ (or $\mathbf{X}$), which is carried out numerically. We want to point out that we have reduced the evaluation of the matrix element to that which we would have obtained for a stripping interaction of the simple form $V=C'\delta^3(\xi)$. However, our derivation allows one to obtain the value of C'. Furthermore, we note that we did not assume a point interaction, nor a point He^3 particle, although we did have to neglect some of the structure effects in the distorted scattered wave functions. One reason for our extensive derivation was to make clear under what conditions one can expect Eq. (37) to be valid. In particular, it requires the radius of the incident particle (He^3) to be small compared to that of the target (nucleus) and also a relevant momentum ($\mathbf{k}$ or $\mathbf{q}$) to be small compared to the average momentum of a nucleon in the incident particle.

III. RESULTS OF THE DISTORTED-WAVE CALCULATIONS

A. Calculation Procedure

The matrix $\mathfrak{M}_J'$, Eq. (37b), is evaluated by expanding the distorted wave functions into partial waves and

[27] This assumes that the dominant Fourier components of χ_k^- are those with momenta close to $\mathbf{k}$, because the main contribution to $\mathfrak{M}_J$ comes from outside the nucleus.

first performing the trivial angular integrations. We choose **K** as the axis of quantization, so that

$$\chi_{\mathbf{K}}^{-}\left(\frac{A}{A+2}\mathbf{R}\right)=\sum_{Lm}\frac{A+2}{A}\frac{4\pi}{kR}i^{L}U_{kL}^{-}\left(\frac{A}{A+2}R\right)\times Y_{L}^{m}(\mathbf{R})Y_{L}^{m*}(\theta,\phi), \quad (39a)$$

$$\chi_{\mathbf{K}}^{+}(\mathbf{R})=\sum_{L'}\frac{1}{KR}i^{L'}[4\pi(2L'+1)]^{1/2}\times U_{KL'}^{+}(R)Y_{L'}^{0}(\mathbf{R}), \quad (39b)$$

where θ, ϕ are the scattering angles and **R** is the variable of integration. The radial wave $i^{L}U_{kL}^{\pm}/kR$ satisfies outgoing (+) or ingoing (−) boundary conditions and

$$U_{kL}^{-*}(R)=U_{kL}^{+}(R); \quad (40)$$

this follows directly from time reversal.[28] With $\phi_{NJ}^{M}(\mathbf{R})=\mathfrak{R}_{NJ}(R)Y_{J}^{M}(\mathbf{R})$, we thus obtain for $\mathfrak{M}_{J'}$,

$$\mathfrak{M}_{J'}=\frac{4\pi}{Kk}\frac{A+2}{A}\times\sum_{LL'}\left[\int\mathfrak{R}_{NJ}(R)U_{kL}^{+}\left(\frac{AR}{A+2}\right)U_{KL'}^{+}(R)dR\right]\times[(2J+1)(2L+1)]^{1/2}\times(JLM-M\,|\,L'0)(JL00\,|\,L'0)i^{L-L'}Y_{L}^{M}(\theta,\phi). \quad (41)$$

The numerical program used on the IBM 709 performs the integration in Eq. (41) and calculates a quantity D_J,

$$D_J=\sum_{M=-J}^{J}|\mathfrak{M}_{J'}|^2. \quad (42)$$

In terms of D_J, the cross section for the (He^3,n) reaction becomes [see Eqs. (34) and (37)]

$$\frac{d\sigma}{d\Omega}=\pi^4V_0^2N_{\mathrm{He}}{}^2\mu_i\mu_f\frac{k}{K}\frac{2J_f+1}{2J_i+1}\times(t_i1\nu_i1\,|\,t_f\nu_f)^2G\sum_{J}\frac{D_JW_J}{2J+1}, \quad (43a)$$

with

$$W_J=|\sum_{j_1j_2}B(j_1j_2J,J_iJ_f)T^{\dagger}(j_1j_2J,J0J)\times H(n0NJ,n_1l_1n_2l_2,J)|^2, \quad (43b)$$

and

$$G=\left|\sum_{j=0}^{n-1}(-1)^jC_{nj}\left(\frac{\alpha^2}{2}\right)^j\frac{\partial^j}{(\partial f^2)^j}\frac{1}{f^3}\frac{1}{g^3}\right|^2. \quad (43c)$$

For $n=1$, G reduces to

$$G=(\alpha^2/2\pi)^{3/2}(1/f^6g^6). \quad (43d)$$

[28] G. Breit and H. A. Bethe, Phys. Rev. **93**, 888 (1954); E. M. Henley and B. A. Jacobsohn, Phys. Rev. **113**, 225 (1959); L. C. Biedenharn, Nucl. Phys. **10**, 620 (1959).

The oscillator radial functions $\mathfrak{R}_{NJ}(R)$ are generated by a subroutine. This makes it easy to generalize the program for other direct reactions. The distorted waves are computed with the UCLA SCAT-4 code,[29] which is slightly altered to give normalized wave functions as output. This program solves the following Schrödinger radial equation

$$\left[-\frac{d^2}{dr^2}+\frac{l(l+1)}{r^2}-k^2+\frac{2\eta k}{r}+2\mu V(r)\right]U_{kl}(r)=0, \quad (44)$$

where μ is the reduced mass of the projectile. It should be noted that the code includes the Coulomb potential; $\eta=\mu Zze^2/k$ is the relevant Coulomb parameter in Eq. (44). The complex nuclear optical potential V can take on a number of forms and can include a spin-orbit term. As stated earlier, we have put this term equal to zero for several reasons. The first of these is that even the optical parameters of the central potential for He^3 elastic scattering are not well known, and the second one is that the spin-orbit effects are most important for large momentum transfers or in the back hemisphere. On the basis of elastic scattering and reaction cross-section analyses made to date, we have chosen the Saxon form for both the real and imaginary parts[30] of the optical potential of He^3,

$$V_{\mathrm{He}}(r)=-(V_1+iV_2)\{1+\exp[(r-R_1)/a_1]\}^{-1}. \quad (45)$$

The same radial dependence (but with different constants) was chosen for the real part of the neutron potential, but the imaginary part was taken to be a Gaussian concentrated at the nuclear surface,[31]

$$V_n(r)=-V_3\{1+\exp[(r-R_3)/a]\}^{-1}-iV_4\exp\{-[(r-R_2)/b]^2\}. \quad (46)$$

We have not attempted to adjust the real parameters of Eqs. (45) and (46), but have used "best-fit parameters" obtained heretofore. The actual values chosen and references are detailed in Table II.

Numerical results are obtained for $\beta^2=0.4$ F^{-2} and $V_0=70$ MeV, which are consistent with the deuteron binding energy. The cross section depends on these parameters primarily through the combination $(V_0/\beta^3)^2$; thus, roughly the same cross section is found for different V_0 and β if V_0/β^3 is kept constant.

The only free parameter that now appears in D_J is the natural frequency of the harmonic oscillator ω that we have kept as a variable. The value of ω obtained from binding energy and nuclear size considerations is

[29] M. A. Melkanoff, J. S. Nodvik, D. S. Saxon, and D. G. Cantor, *A Fortran Program for Elastic Scattering Analyses with the Nuclear Optical Model* (University of California Press, Berkeley, California, 1961).

[30] For a strongly absorbed particle, we have found that the choice between surface and volume absorption is not as important as for weakly absorbed ones.

[31] F. Bjorklund and S. Fernbach, Phys. Rev. **109**, 1295 (1958).

TABLE II. Values of optical potential parameters. Energies are given in units of MeV and radii in Fermis; $R_{i0}=R_iA^{-1/3}$.

Parameters \ Target	C^{12}	O^{16}	Ni	Sn	References
V_1	55	55	30	30	P. E. Hodgson, *Proceedings of the Rutherford Jubilee International Conference, Manchester, 1961* (Academic Press Inc. New York, 1961), p. 407
V_2	60	60	25	18	
R_{10}	1.6	1.6	1.6	1.6	
a_1	0.6	0.6	0.61	0.5	
V_3	43	43	42	42	
V_4	12	12	12.5	12.5	
R_{20}	1.25	1.25	1.25	1.25	Ref. 31
R_{30}	1.25	1.25	1.25	1.25	
a	0.65	0.65	0.65	0.65	
b	0.98	0.98	0.98	0.98	

$41A^{-1/3}$ MeV.[32] However, we need primarily the bound-state wave functions close to and outside the nuclear surface, since the overlap with the initial- and final-state wave functions (χ_i^+,χ_f^-) is small inside the nucleus.[33] Thus, one way of determining ω is to compare the harmonic-oscillator single-particle wave function close to the nuclear surface with that of a particle bound in a finite Saxon well. We have adopted this procedure and make the comparison with the ground-state wave function of a single particle. The binding energy of the latter is taken to be the average separation energies of a proton from the nuclei $A+2$ (final nucleus) and $A+1$. For the targets that we consider, the values of ω so determined are always close to 3 MeV, which is generally considerably less that $41A^{-1/3}$. A reduced value of ω is, however, also suggested by the treatment of Sec. IIC. Furthermore, residual nucleon-nucleon forces tend to lower the energies of single-particle states. For excited states of the final nucleus, even the adjusted value of ω may be too large, since the tail of the corresponding wave functions fall off even more slowly than that of the ground state. Since we find that the shapes of the differential cross sections are not sensitive to small variations of ω (unlike the ratios of cross sections to various final states), the same ω is kept for all final states.

B. Transitions to Definite Final States

1. $C^{12}(He^3,n)O^{14}$

We shall restrict our comparison with experiments to incident energies close to 20 MeV.[3,34] Although the experimental level structure of O^{14} is not too well known, considerable lore exists about the corresponding $T=1$ states in N^{14}.[35] In the first two columns of Table III are summarized the energies and spins of the low-lying known $T=1$ levels of N^{14}; in the third column the energies (approximate, where not measured) of the corresponding levels in O^{14} are listed.[35] The energies not measured were obtained by simply placing the lowest $T=1$ state of N^{14} at zero energy.

There have also been a large number of theoretical studies of the structure of the N^{14} (and O^{14}) nucleus.[36] The recent one by True[36] indicates that many of the low-lying levels can be accounted for by treating C^{12} as

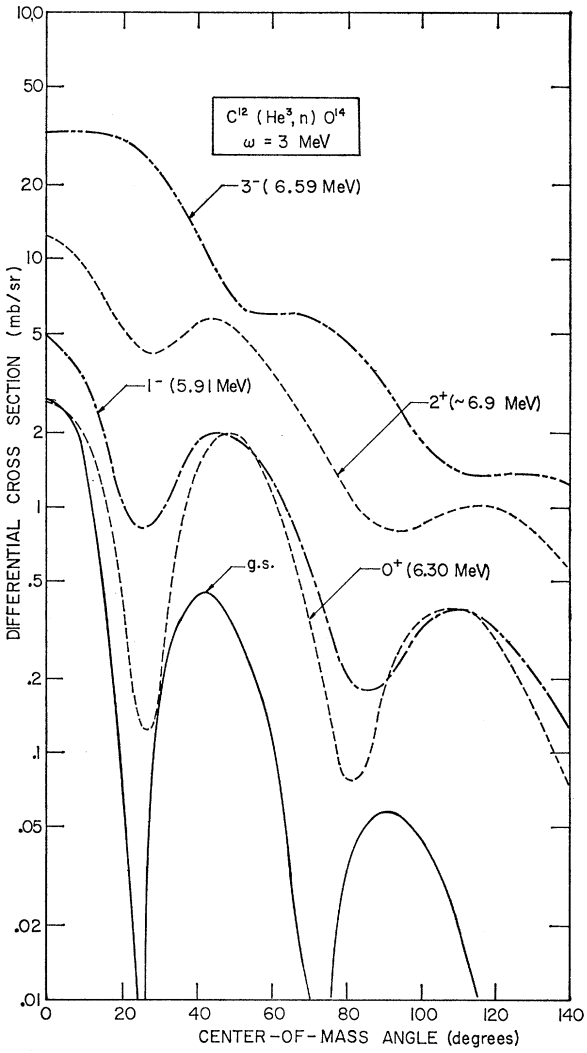

FIG. 3. Differential cross sections for the $C^{12}(He^3,n)O^{14}$ reaction at 20 MeV for various final states. Spectroscopic weights for the various final states are determined from the wave functions suggested by True (see Table III). The harmonic oscillator energy spacing ω is 3 MeV.

[32] S. G. Nilsson, Kgl. Danske Videnskab. Selskab, Mat. Fys. Medd. **29**, No. 16 (1955).

[33] We have compared D_J without and with radial cutoffs (at 3F and 5F, for C^{12}) and find only minor differences.

[34] Experiments at lower energies are summarized by R. Middleton, in *Proceedings of the International Symposium on Direct Interaction and Nuclear Reaction Mechanisms, Padua, 1962* (Gordon and Breach, Publishers, New York, 1963), p. 435.

[35] T. Lauritsen and F. Ajzenberg-Selove, *Energy Levels of Light Nuclei* (National Academy of Sciences—National Research Council, Washington, D. C., 1962).

[36] W. W. True, Phys. Rev. **130**, 1530 (1963). References to earlier work are contained in this paper.

TABLE III. Energy-level spin assignments and spectroscopic factors for O^{14}. Spin assignments and energies of the low-lying $T=1$ states of N^{14} are given in columns 1 and 2. Experimentally determined or approximate theoretical energies of the corresponding levels in O^{14} appear in column 3. In columns 4 and 5 are listed the pure shell configurations and their corresponding spectroscopic weights, W_J. The configuration assigned by True (Ref. 36) and the corresponding W_J appear in columns 6 and 7. Principal quantum numbers are omitted for the sake of brevity in these last columns.

State spin and parity	Energy (MeV) in N^{14} exper. (theor.)	(Approximate) energy in O^{14} (MeV)	Pure shell configuration	W_J	True configuration	W_J
0^+	2.31 (2.72)	0	$(1p_{1/2})^2$	0.167	$-0.9501p_{1/2}^2+0.1219s_{1/2}^2$ $+0.2635d_{5/2}^2+0.1139d_{3/2}^2$	0.048
1^-	8.06 (6.99)	5.91	$(1p_{1/2}2s_{1/2})$	0.138	$-0.9945p_{1/2}s_{1/2}$ $+0.1050p_{1/2}d_{3/2}$	0.164
0^+	8.63 (7.91)	6.30	$(2s_{1/2})^2$	0.208	$-0.2056p_{1/2}^2-0.936s_{1/2}^2$ $-0.2754d_{5/2}^2-0.076d_{3/2}^2$	0.382
0^-	8.71 (8.12)	(6.40)	$(1p_{1/2}2s_{1/2})$	0	$p_{1/2}s_{1/2}$	0
3^-	8.91 (7.43)	6.59	$(1p_{1/2}1d_{5/2})$	0.250	$p_{1/2}d_{5/2}$	0.250
2^+	9.17 (?)	(6.86)			core excitation	
2^-	9.51 (8.99)	(7.20)	$(1p_{1/2}1d_{5/2})$	0	$-0.9997p_{1/2}d_{5/2}$ $+0.0260p_{1/2}d_{3/2}$	0
2^+	10.42 (9.57)	(8.11)	$(2s_{1/2}1d_{5/2})$	0.1750	$-0.8981s_{1/2}d_{5/2}+0.1003d_{3/2}d_{5/2}$ $-0.3599d_{5/2}^2-0.2219s_{1/2}d_{3/2}$ $-0.0675d_{3/2}^2$	0.300
0^+	11.23 (10.49) (?)	(8.92)	$(1d_{5/2})^2$	0.100	$-0.2262p_{1/2}^2+0.3278s_{1/2}^2$ $-0.9063d_{5/2}^2-0.1414d_{3/2}^2$	0.071
2^+	~12 (11.95)	(~9.7)	$(1d_{5/2})^2$	0.0400	$-0.3857s_{1/2}d_{5/2}+0.9163d_{5/2}^2$ $+0.0171s_{1/2}d_{3/2}-0.0920d_{3/2}d_{5/2}$ $+0.0535d_{3/2}$	0.0024
4^+	~12.8 (11.94)	(~10.5)	$(1d_{5/2})^2$	0.0750	$-0.9636d_{5/2}^2$ $+0.2674d_{3/2}d_{5/2}$	0.168

an inert core; the exceptional low-lying level of O^{14} that appears to require core excitation is the 2^+ state at approximately 6.9 MeV. In addition, it is expected that the ground state has some admixture of core excitations, because of its $(1p_{1/2})^2$ configuration. In our work, core excitation has been neglected because we anticipate that the cross section to such states, and thus to the 2^+ state at ~6.9 MeV, is small. In the 4th and 5th columns of Table III we list the pure shell assignments of the various levels of O^{14} and the relevant weighting factors W_J. In the last two columns we give the assignment suggested by True[36] (calculated with inclusion of particle-particle forces), together with the spectroscopic weighting factors. In this case W_J involves a sum over j_1 and j_2 before squaring. It should be noted that considerable configuration mixing is present. This has the effect of reducing the expected single-particle transition rate to the ground state by a factor of almost three, but also enhancing that of the O^+ excited states by roughly the same factor. Of the three 2^+ states in O^{14} below 10 MeV, only the one at ~8 MeV has an associated large weighting factor.

In order to obtain absolute magnitudes for the cross sections to various final states of O^{14} we also need to evaluate the overlap integral over the relative coordinate of the two captured protons, represented by G, Eq. (43c). This overlap depends on the choice of the harmonic oscillator frequency. For the "normal" value[32] of $\omega=41/A^{1/3}$ ($\approx$17–18 MeV for C^{12}), we note that $\alpha^2\approx3\gamma^2$. As pointed out earlier, the overlap of the $nl=n0$ state of the harmonic oscillator with the internal He^3 wave function is then equal to zero unless $n=1$; thus only the $j=0$ term contributes and G is given by Eq. (43d). Although we have adjusted the frequency ω to correspond roughly to the single-particle wave function at the nuclear surface, we shall assume that only the $n=1$ state contributes to the cross section.

The calculated absolute differential cross sections to the ground state, to the 1^-, 0^+ ($\approx$6.32 MeV), 3^- and 2^+ ($\approx$8.11 MeV) states are plotted in Fig. 3 for $\omega=3$ MeV and in Fig. 4 for $\omega=5$ MeV. The comparison of the harmonic oscillator wave functions of a $1p$ state for different ω with that of a single particle bound in a finite well with an energy of 3.5 MeV is made in Fig. 5. Examination of this figure shows why we used 3 and 5 MeV for the determination of absolute cross sections. Comparisons of Figs. 3 and 4 shows that although the angular distributions are quite insensitive to the change of ω, the absolute magnitudes of the cross sections and the ratios of these to various final states are quite sensitive to this change. Note, in particular, the enhancement of the highest angular momentum (3^-) state when ω is reduced. This appears to be a fairly general feature, which we also noted for other target nuclei.

A comparison of our calculated angular distribution for the ground state transition with that measured by J. H. Manley[3] is shown in Fig. 6. It is only for $\omega\lesssim5$ MeV that a reasonable fit to the measured differential cross section obtains; for $\omega=5$ MeV the calculated cross section at 0° is 1.3 mb/sr, and for $\omega=3$ MeV it is 2.7 mb/sr. These compare favorably with the 3.4 mb measured by Manley.[3] It should be noted that it is not only the angular distribution that requires $\omega\lesssim5$ MeV, but the absolute magnitude of the differential

cross section as well. In Fig. 7 we plot theoretical relative differential cross sections for the ground state transition with $\omega=3$, 5, 8, 12, and 16 MeV. It is seen that an increase of the harmonic oscillator frequency drastically reduces the magnitude of the cross section. Physically, this arises because the bound-state wave function at and beyond the nuclear radius is reduced by a larger oscillator frequency, and it is in this region that most of the contribution to D_J arises.

In order to further compare results obtained with the infinite harmonic oscillator to those for a finite potential we have carried out a calculation of the angular distribution expected for two protons captured at the same point into $1p_{1/2}$ states of a finite Saxon-type well. The depth of this well is adjusted to give the average of the separation energies of the last proton in N^{13} and O^{14} ($\approx$3.5 MeV). The comparison in Fig. 8 shows excellent agreement.

In Fig. 6 also appears the plane-wave result for the ground-state transition with a radius of 4.8 F, chosen

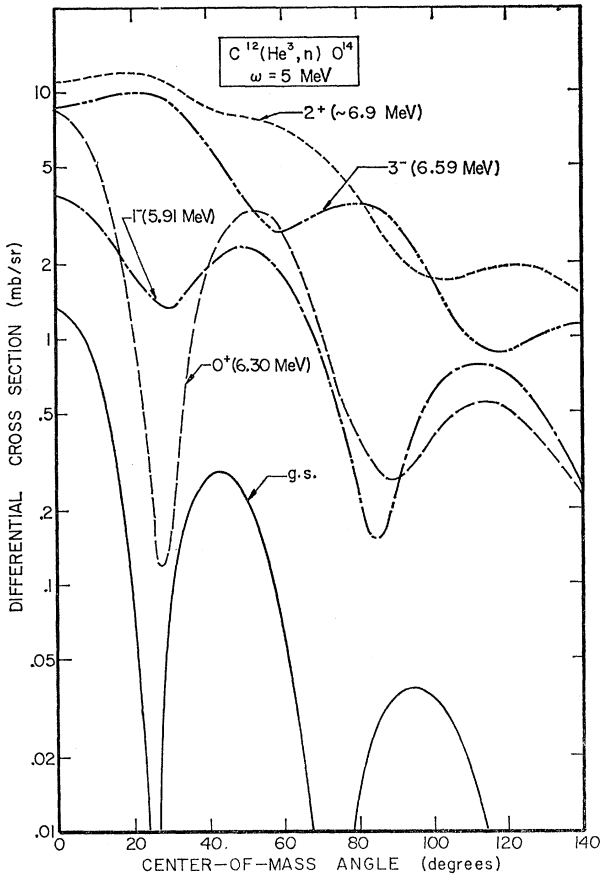

FIG. 4. Differential cross sections for the $C^{12}(He^3,n)O^{14}$ reaction at 20 MeV for various final states. Spectroscopic weights for the various final states are determined from the wave functions suggested by True (see Table III). The harmonic oscillator energy spacing ω is 5 MeV.

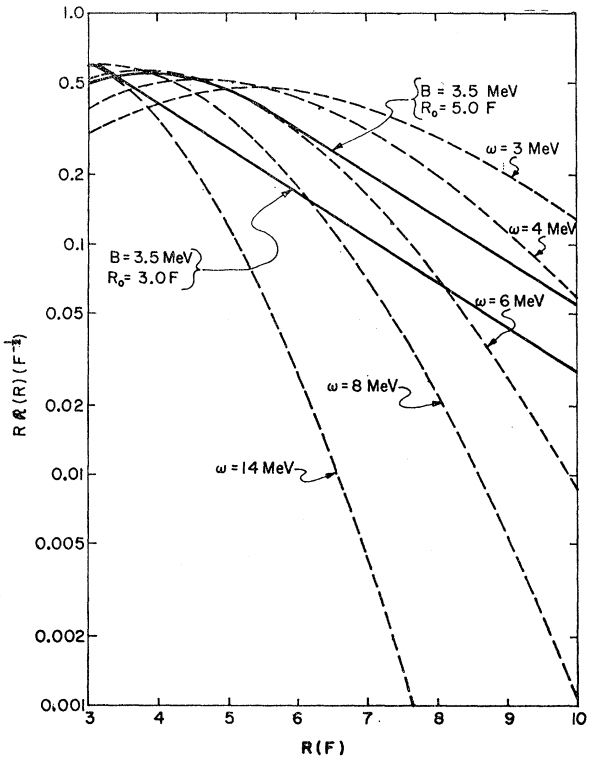

FIG. 5. Comparison of the single-particle harmonic oscillator wave function with that of a nucleon bound in a finite Saxon well. The dashed lines correspond to different values of the harmonic oscillator frequency ω. The solid curves are those for a nucleon bound with an energy $B=3.5$ MeV in a Saxon potential of radius R_0, and fall-off distance of 0.5 F.

to fit the calculated maximum at 42° and the minimum at 73°; it is seen that the nuclear distortions are important. As already pointed out by Manley,[3] it is not possible to choose a reasonable radius which fits the position of the first maximum (beyond zero) and also gives a forward peak.

2. $O^{16}(He^3,n)Ne^{18}$

The calculations of the cross sections for an O^{16} nuclear target are similar to those for C^{12}, except that states which involve a $p_{1/2}$ configuration are absent in Ne^{18}. The energies and spins of the levels of the mirror nucleus to Ne^{18}, namely O^{18}, have recently been studied in detail.[37] In Table IV we list the known low-lying levels of O^{18} together with the corresponding levels in Ne^{18}. Since the energy comparisons are close, where known, we assume approximately the same level spins and energies as in O^{18} where these are not known in Ne^{18}. The configurations of the low-lying states of O^{18} or Ne^{18} have not been studied as extensively as those of the $A=14$ nuclei. In the 4th and 5th columns of Table IV we list the expected dominant shell configura-

[37] A. E. Litherland, R. Batchelor, A. J. Ferguson, and H. E. Gove, Can. J. Phys. 39, 276 (1961).

TABLE IV. Energy-level spin assignments and spectroscopic factors for Ne^{18}. The spin assignments (where known) and energies of low-lying levels of O^{18} are given in columns 1 and 2. The corresponding energies of known levels in Ne^{18} are given in column 3. In the 4th column are listed pure-shell model configurations, based on the N^{14} studies of Table I. In column 6 appear the configurations predicted by Elliott (Ref. 39) on the basis of the U_3 classification scheme (principal quantum numbers have been omitted). Corresponding spectroscopic weights are listed in columns 5 and 7.

State spin and parity[a]	Energy in O^{18} [a] (MeV)	Energy in Ne^{18} [b] (MeV)	Possible shell-model assignment	W_J	Elliott[c] U_3 scheme (LS coupling)	W_J
0^+	0	0	$(2s_{1/2})^{1/2}$	0.208	$(5/9)^{1/2}s^2+(4/9)^{1/2}d^2$	0.374
2^+	1.98	1.88	$(2s_{1/2}1d_{5/2})$	0.175	$(7/9)^{1/2}ds-(2/9)^{1/2}d^2$	0.404
4^+	3.55	3.36	$(1d_{5/2}1d_{5/2})$	0.075	d^2	0.374
0^+	3.63	3.61	$(1d_{5/2})^2$	0.100	$(4/9)^{1/2}s^2-(5/9)^{1/2}d^2$	0
2^+	3.92				$(2/9)^{1/2}s^2+(7/9)^{1/2}d^2$	0.112
	4.45					
	5.01					
	5.17					
	5.31					
	5.46					
	6.19					
	6.33					
4^+	7.13					
1^-	7.63					
1^-	8.05					
2^+	8.22					
3^-	8.29					
	8.41					
	8.83					
	8.97					

[a] See Ref. 37. [b] See Ref. 35. [c] See Ref. 39.

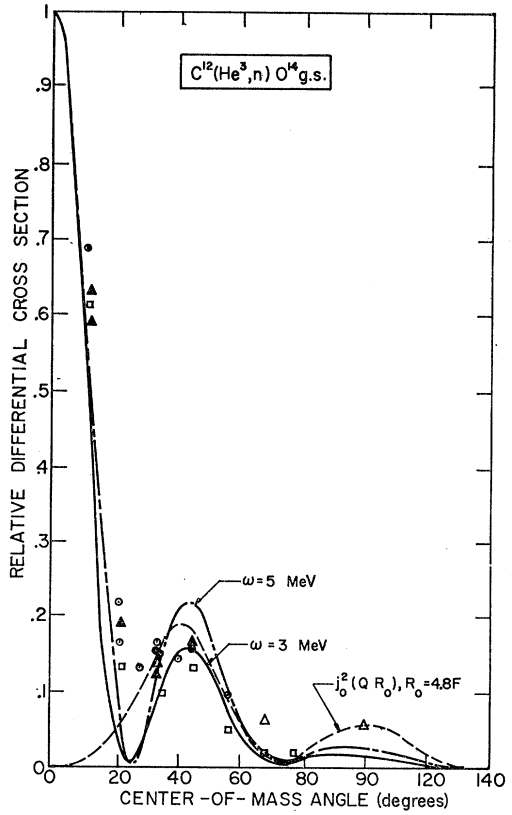

FIG. 6. Comparison of experimental and theoretical differential cross sections for the $C^{12}(He^3,n)O^{14}$ g.s. reaction. The experimental points (□, △, ▲, ○, ●) are those of J. H. Manley (see Ref. 3). Theoretical curves are shown for both $\omega=3$ MeV and $\omega=5$ MeV, as well as for the plane-wave Born approximation, arbitrarily normalized.

tion, based on the $A=14$ study of True.[36] The effects of particle-particle residual forces have been studied by Redlich,[38] by Elliott,[39] and by Elliott and Flowers[40] mainly in L-S coupling; O^{18} is argued to be close to this limit. According to Elliott and Flowers' intermediate coupling study,[40] the ground-state configuration in L-S coupling is (see Ref. 40 for notation)

$$\psi_0=0.84(d^2)^{31}S-0.38(d^2)^{33}P+0.39(s^2)^{31}S; \quad (47)$$

for j-j coupling they obtain

$$\psi_0=0.89(d_{5/2})^2+0.24(d_{3/2})^2+0.39(s_{1/2})^2. \quad (48)$$

In both cases W_J is 0.272. In a further paper,[39] Elliott discusses the U_3 scheme of classifying the O^{18} levels. In that case the configurations (in L-S coupling) and their spectroscopic weights are given in columns 6 and 7 of Table IV. It should be noted that intermediate coupling predicts a predominantly d^2 configuration for the ground state of Ne^{18}, whereas the U_3 scheme slightly prefers the s^2 configuration. In Fig. 9 we plot the predicted absolute differential cross section to the ground state and to the first excited 2^+ and 4^+ states for $\omega=3$ MeV. This choice of ω is determined as for C^{12}. Again we use Eq. (43d) for G. The spectroscopic weights of the last column of Table IV are employed.

3. $Ni^{58}(He^3,n)Zn^{60}$

The target nucleus Ni^{58} has a closed $1f_{7/2}$ proton shell. The level structure of the final nucleus has not

[38] M. G. Redlich, Phys. Rev. **95**, 448 (1954).
[39] J. P. Elliott, Proc. Roy. Soc. (London) **A245**, 128, 562 (1958).
[40] J. P. Elliott and B. H. Flowers, Proc. Roy. Soc. (London) **A229**, 536 (1955).

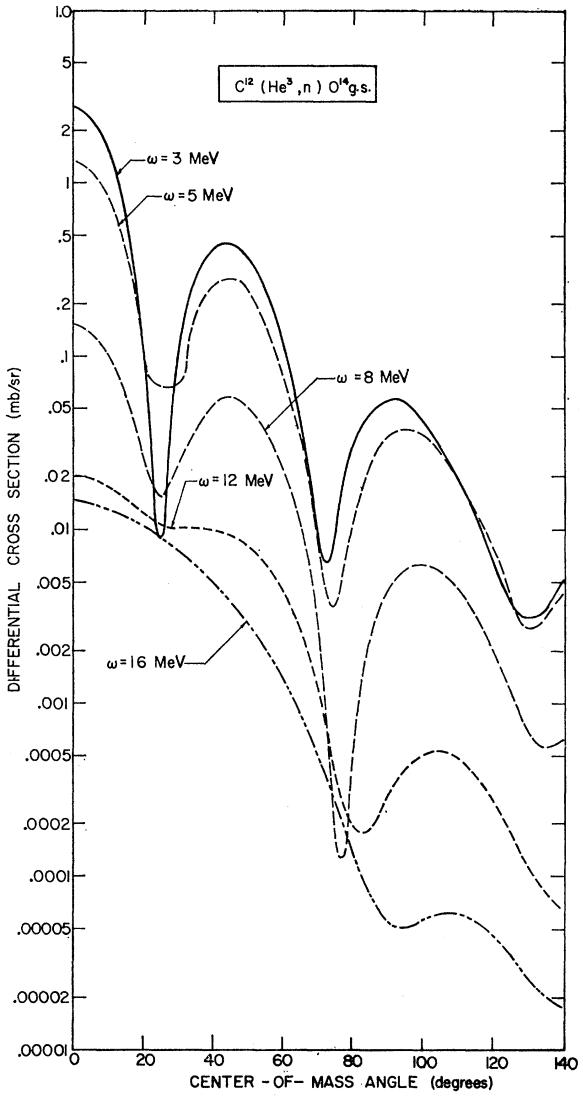

FIG. 7. Comparison of calculated differential cross sections for the $C^{12}(He^3,n)O^{14}$ g.s. reaction with different values of the harmonic oscillator energy spacing ω.

been extensively investigated. In Table V, we list possible pure shell configurations and their relevant spectroscopic weights. However, it is known that residual nucleon-nucleon forces are important and that these give rise to considerable configuration mixing. We can use the wave functions suggested by Kisslinger and Sorenson[41] to obtain a better estimate of the ground-state transition spectroscopic weight. For this purpose, we neglect proton-neutron interactions and take their wave function for two nucleons in the lowest unfilled "major shell" $(2p_{3/2},2p_{1/2},1f_{5/2},1g_{9/2})$. As shown by Yoshida,[1] the spectroscopic factor B is given by

$$B=\sum_{j_1}(j_1+\tfrac{1}{2})^{1/2}U_{j_1}(\mathrm{Ni})V_{j_1}(\mathrm{Zn}), \qquad (49)$$

[41] L. S. Kisslinger and R. A. Sorensen, Kgl. Danske Videnskab. Selskab, Mat. Fys. Medd. **32**, No. 9 (1960).

TABLE V. Spectroscopic weights for the excitation of even-parity single-particle states in the $Ni(He^3,n)Zn$ reaction.

State spin and parity	Pure shell configuration	W_J
0^+	$2p_{3/2}2p_{3/2}$	0.175
0^+	$1f_{5/2}1f_{5/2}$	0.021
0^+	$2p_{1/2}2p_{1/2}$	0.088
2^+	$2p_{3/2}2p_{3/2}$	0.053
2^+	$2p_{3/2}1f_{5/2}$	0.013
2^+	$1f_{5/2}1f_{5/2}$	0.007
2^+	$2p_{3/2}2p_{1/2}$	0.105
2^+	$1f_{5/2}2p_{1/2}$	0.045
4^+	$2p_{3/2}1f_{5/2}$	0.118
4^+	$1f_{5/2}1f_{5/2}$	0.008

where U and V are determined by the Bogoliubov-Valatin[42] transformation and can be found from the tables of Kisslinger and Sorensen. (The relevant parameters are $\lambda=-0.31$ MeV, $\Delta=0.80$ MeV.[41]) With this prescription, we find that the spectroscopic weight

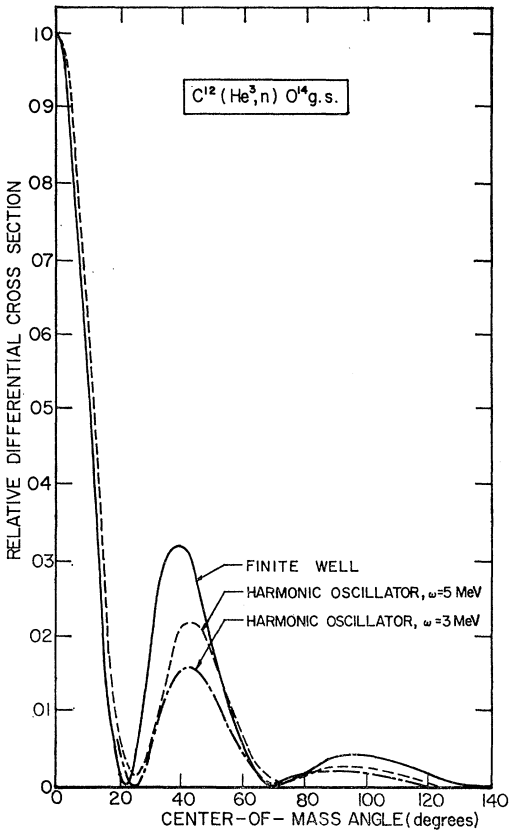

FIG. 8. Comparison of calculated differential cross section for the $C^{12}(He^3,n)O^{14}$ g.s. reaction for different bound-state wave functions. Those labeled by $\omega=3$ MeV and $\omega=5$ MeV employ harmonic oscillator functions, whereas that indicated by "finite well" is for the capture of two protons at the same point in a Saxon potential.

[42] N. N. Bogoliubov, Zh. Eksperim. i Teor. Fiz. **34**, 58, 73 (1958) [English transl.: Soviet Phys.—JETP **7**, 41, 51 (1958)]; J. G. Valatin, Nuovo Cimento **7**, 794 (1958).

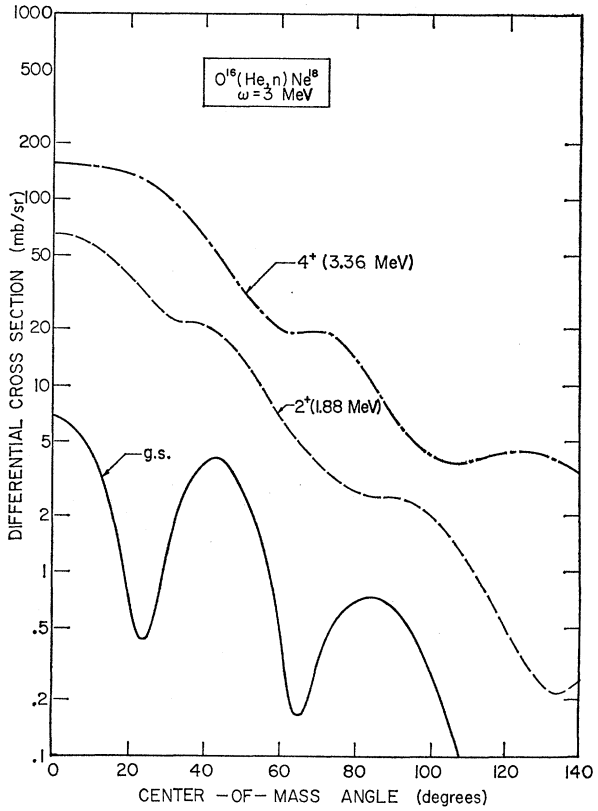

FIG. 9. Calculated differential cross sections for the $O^{16}(He^3,n)$-Ne^{18} transition at 20 MeV for various final states. Spectroscopic weights are given in the last column of Table IV.

W_J for the ground-state transition is 0.22; comparison with Table V brings out the enhancement due to the configuration mixing. In Fig. 10 we plot the differential cross section for 20-MeV He^3 ions to the ground state, based on the above spectroscopic factor, and compare it to the Born approximation. For simplicity, we have again dropped all but the $j=0$ term in the sum of Eq. (43c). Our criterion for ω yields, with a binding energy of 6.9 MeV, a value between 3 and 4 MeV. We have used $\omega=3$ MeV in computing the cross section.

4. $_{50}Sn^{120}(He^3,n)_{52}Te^{122}$

Tin has a closed proton $1g_{7/2}$ state, but several isotopes are known to be stable. The pure shell spectroscopic factors for even parity final states of $J\leq 4$ are listed in Table VI. We shall not use these for the ground-state transition, but rather consider the Kisslinger-Sorenson[41] pairing model, neglecting neutron excitations. For two nucleons in the $2d_{5/2}$, $1g_{7/2}$, $3s_{1/2}$, $2d_{3/2}$, $1h_{11/2}$ shells, their tables suggest $\Delta\approx 0.80$ MeV, $\lambda\approx -0.80$ MeV. With these values and use of Eq. (49), we find 0.129 for the spectroscopic factor W_J to the 0^+ ground state (of any even isotope of Te). Comparison with Table VI again brings out the enhancement of the spectroscopic factor for this transition. Figure 11 shows the differential cross section to the ground state of Te^{122} for 20-MeV He^3 ions; the unnormalized Born approximation cross section also ap-

TABLE VI. Spectroscopic weights for excitation of even-parity single-particle states with a Sn target.

State	Pure shell assignment	Pure shell W_J
0^+	$2d_{5/2}2d_{5/2}$	0.096
0^+	$1g_{7/2}1g_{7/2}$	0.006
0^+	$2d_{3/2}2d_{3/2}$	0.064
0^+	$3s_{1/2}3s_{1/2}$	0.099
2^+	$2d_{5/2}2d_{5/2}$	0.030
2^+	$1g_{7/2}1g_{7/2}$	0.002
2^+	$1g_{7/2}2d_{5/2}$	0.002
2^+	$1g_{7/2}2d_{3/2}$	0.020
2^+	$2d_{5/2}2d_{3/2}$	0.015
2^+	$2d_{5/2}3s_{1/2}$	0.093
2^+	$2d_{3/2}2d_{3/2}$	0.018
2^+	$2d_{3/2}3s_{1/2}$	0.062
4^+	$2d_{5/2}2d_{5/2}$	0.027
4^+	$1g_{7/2}1g_{7/2}$	0.002
4^+	$1g_{7/2}2d_{5/2}$	0.011
4^+	$1g_{7/2}2d_{3/2}$	0.014
4^+	$1g_{7/2}3s_{1/2}$	0.033
4^+	$2d_{5/2}2d_{3/2}$	0.109

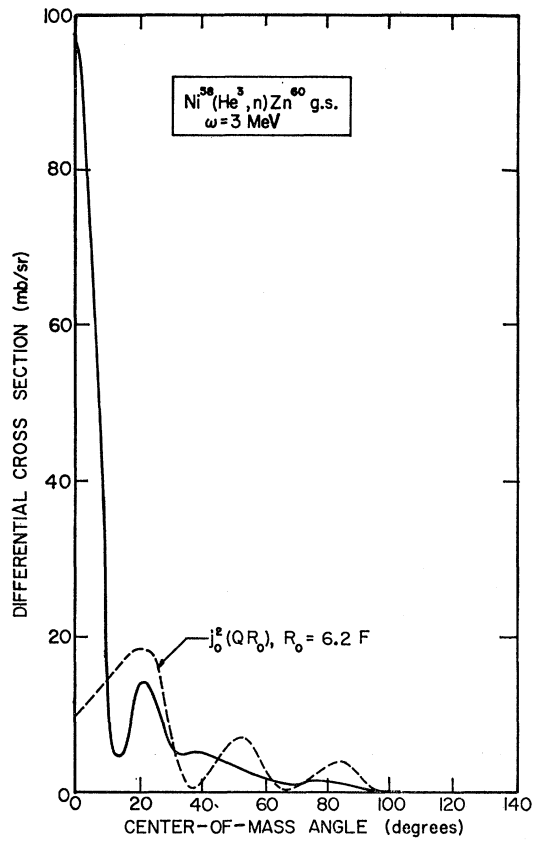

FIG. 10. Calculated differential cross section for the $Ni^{58}(He^3,n)$-Zn^{60} g.s. reaction at 20 MeV. The dashed curve is the plane-wave Born approximation angular distribution, arbitrarily normalized.

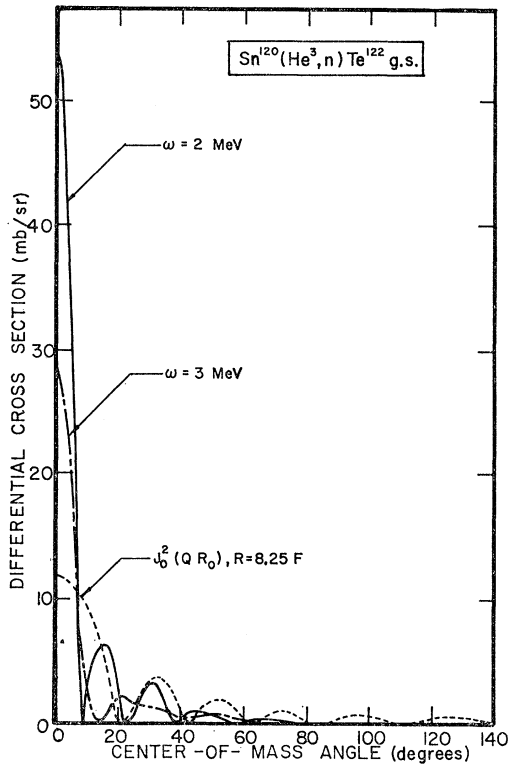

FIG. 11. Calculated differential cross section for $Sn^{120}(He^3,n)Te^{122}$ g.s. transition at 20 MeV for both $\omega=2$ and 3 MeV. The dashed curve is the plane-wave Born approximation angular distribution, arbitrarily normalized.

pears. Cross sections are presented for both $\omega=3$ MeV and $\omega=2$ MeV; these values are justified as before. The 0° cross section is enhanced, and the width of the major peak in the angular distribution is reduced by decreasing ω from 3 to 2 MeV.

C. Comparison to Threshold Detector Experiments

When a threshold detector is used to detect the final neutrons, the measured cross section is that to the ground state and all excited states up to a maximum excitation energy. It is thus the sum of the cross sections to the low-lying final states discussed in Sec. III B. One possible advantage of such measurements is that the differential cross section should be less dependent on the nuclear angular momenta and more so on other features involved, such as the distortion of the incident He^3 and outgoing neutron wave. A semiclassical model, based on these considerations, is developed in Sec. IV. As remarked earlier, in Born approximation, a sum of the type $\sum_L j_L^2(QR)$ gives a relatively flat angular distribution. By comparison, angular distributions measured by Manley[43] for all the target nuclei discussed in Sec. III B show a strong forward peaking.

In order to relate our distorted-wave calculation with threshold detector experiments, we assume that all states corresponding to both particles being captured into the next major oscillator shell can be reached. To minimize the computational time, we have taken all of these energies to be identical; that is, we assume that all final states that can be reached are degenerate. In order to test the sensitivity of the results to the energy used, the cross sections for an average excitation energy of ~3 MeV and of 7–10 MeV were compared.

The spectroscopic weights to the available final states are computed by summing over all single-particle states that can lead to the given states; that is $W_J=\sum_{j_1j_2}|BT^\dagger H|^2$, where the sum is over all the accessible single-particle states that lead to the spin J. Thus, the sum is over the single-particle states listed in Tables III–VI for C, O, Ni, and Sn targets, respectively.[44] The results of this summation are given in Table VII.

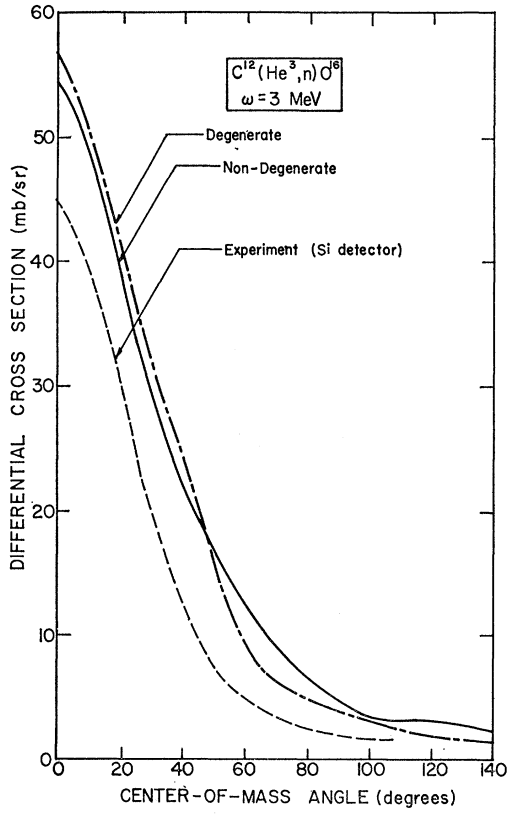

FIG. 12. Summed differential cross sections for the $C^{12}(He^3,n)O^{14}$ reaction. The solid curve is that computed by summing the differential cross sections shown in Fig. 3. The curve labeled "degenerate" is the calculated sum of the differential cross sections, for 20-MeV incident He^3 ions, to 0^+, 2^+, 4^+ states assumed to all lie at 6 MeV excitation. The dashed curve is that obtained by Manley with a Si threshold detector.

[43] J. H. Manley (private communication); and Ref. 3.

[44] A different and considerably more complicated treatment has been suggested by S. Yoshida, Nucl. Phys. (to be published), but we shall not use it here.

TABLE VII. Spectroscopic weighting factors for sum of even J_f low-lying levels. In the table appear the sum of the single-particle weighting factors, for a given J_f, to all of the harmonic oscillator states of the first unfilled major shell. For C^{12}, the $d_{3/2}$ state has not been included because its energy is too high (see Table II). For O^{16} the values outside parentheses are W_J with $d_{3/2}$ states omitted and the values inside parentheses include these states.

Final state J_f	Target C^{12}	O^{16}	Ni	Sn
0^+	0.475	0.308(0.375)	0.284	0.265
2^+	0.215	0.215(0.418)	0.222	0.243
4^+	0.075	0.075(0.375)	0.126	0.197

In Fig. 12 we compare the single-particle-summed differential cross section with experiment[3] and with that obtained by summing the cross sections displayed in Fig. 3 corresponding to states in O^{14} up to 7 MeV with the configurations suggested by True (see Table III). Although the magnitudes of the cross section differ, their angular patterns are similar.

In Figs. 13–15 we show the single-particle-summed differential cross sections for O^{16} ($\omega=3$ MeV), Ni ($\omega=3$ MeV), and Sn ($\omega=3$ MeV and $\omega=2$ MeV) targets for two different average excitation energies. In general, the magnitudes of the cross sections differ for these two energies, but the angular distributions are similar. It is especially noteworthy that all angular distributions are peaked forwards, in agreement with preliminary data.[43] For tin, the cross section reaches a maximum away from 0°. As ω is decreased from 3 to 2 MeV, the ratio of this maximum to the 0° cross section decreases and the angular distribution becomes narrower. With a more realistic method of summing cross sections (e.g., non-degenerate energy levels), it is likely that the forward angle structure that appears in Figs. 14 and 15 would disappear.

In Table VIII we list the angles at which the cross section shown in Figs. 12–15 drop to one-half of their maxima. This angle is almost independent of A for a fixed ω of 3 MeV, except for tin. However, with $\omega=2$ MeV for tin, the half-width is approximately the same as for the other targets studied. The reduction arises because the angular distribution is primarily that for the 4^+ state and this distribution is narrowed by decreasing ω from 3 to 2 MeV. The near constancy of the half-width can be understood as follows: (a) The nuclear

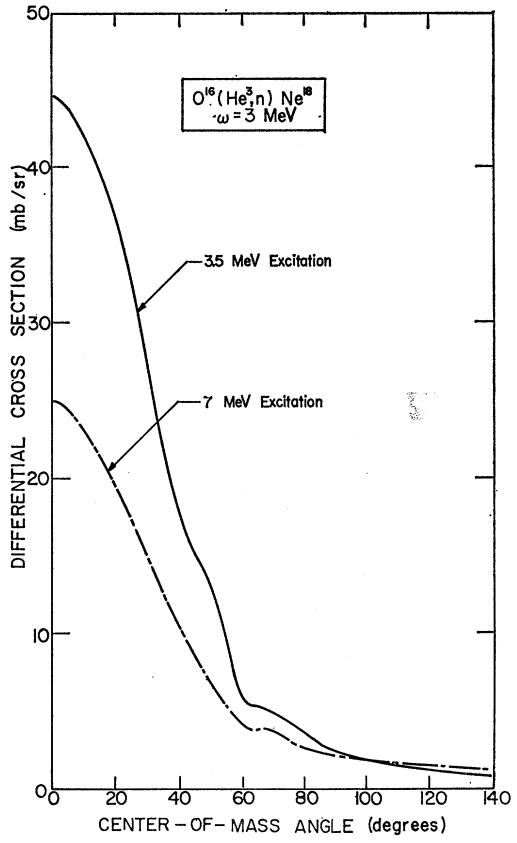

FIG. 13. Calculated summed differential cross sections for the O^{16}(He^3,n)Ne^{18} reaction with 20-MeV He^3 ions to low-lying 0^+, 2^+, and 4^+ states. All states are assumed degenerate at 3.5-MeV excitation for the solid curve and at 7-MeV excitation for the dot-dash curve.

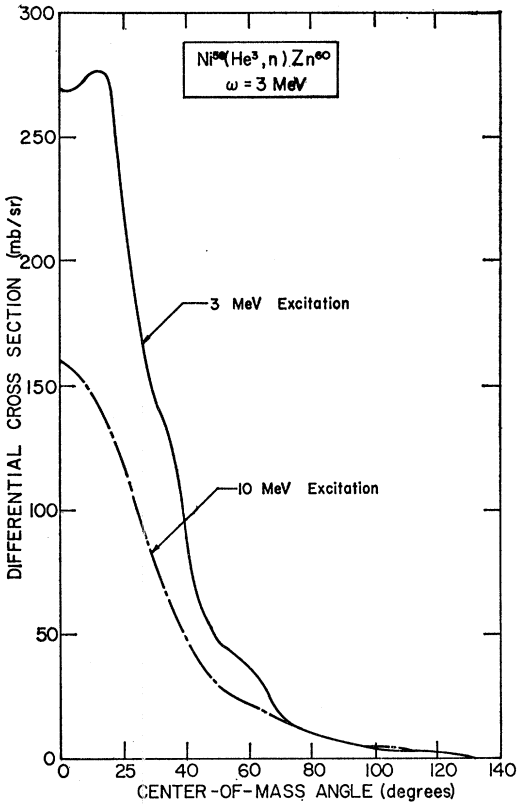

FIG. 14. Sum of cross sections for the excitation of 0^+, 2^+, and 4^+ states by the Ni^{58}(He^3,n)Zn^{60} reaction. The harmonic oscillator spacing is 3 MeV. Differential cross sections for an average excitation energy of 3 and 10 MeV are shown.

TABLE VIII. Half-widths of angular distributions for poor-resolution-type experiments, based on a distorted-wave calculation.

Target	C^{12}	O^{16}	Ni	Sn $\omega=3$ MeV	Sn $\omega=2$ MeV
Half-width (low-excitation energy)	34°	34°	33°	45°	34°
Half-width (high-excitation energy)	···	36°	30°	58°	39°
Half-width (summed cross sections)	34°	···	···	···	···

optical potentials (especially the absorptive parts thereof) for the incoming He^3 and emerging neutron tend to peak all cross sections at 0°, particularly those to 0^+ states. (b) As the atomic weight of the target increases, the larger radii tend to shrink the width of the forward peak, but the Coulomb potential partially offsets this decrease. Furthermore, for the fixed ω that our prescription dictates, the relative cross section for the excitation of higher spin states increases with target weight. Because the angular distribution of these higher J_f states (2^+ and 4^+) becomes wider as A increases, the summed cross section also is broadened. In fact, it is the cross section to these higher states which causes the structure near forward angles in Figs. 14 and 15. We shall see in the next section how these features are reproduced by a simple model.[45]

The tendency to excite higher angular momentum states in two-particle stripping reactions has also been noted in (α,d) stripping at higher energies (47 MeV). For p-shell target nuclei, Harvey *et al.*[46] found that the highest possible spin state $[(d_{5/2})^2$ coupling to $J_f=5]$ is the most strongly populated one. For the (He^3,n) reaction the correspondingly strongly excited final state would be the $J_f=4$ state. For a C^{12} target, the first 4^+ state lies close to the limit of the silicon counters used by Manley.[3] Furthermore, the spectroscopic weighting factors to this state are small (see Tables III and VII) so that no strong excitation of it is predicted. However, Fig. 3 shows that the cross section of the 3^- state indeed dominates over all others. For O^{16} the 4^+ lies lower and the cross section to this state is about $2\frac{1}{2}$ times that to the 2^+ and 0^+ states, even though its spectroscopic weight is not large if $d_{3/2}$ states are omitted (see Table VII).

IV. A SIMPLE DIFFRACTION MODEL

When strong nuclear absorption is present, many of the features exhibited by the distorted-wave calculations of stripping reactions can be understood in terms of a simple diffraction model. The reason for considering an idealized model is twofold. First, it should help us gain clear physical, or intuitive, insights into the pronounced aspects of the situation of interest, such as the angular distribution. Secondly, it may yield simple analytical results which can be readily compared with experiments.

We first point out that in our distorted-wave calculations, the imaginary parts of the optical potentials (see Table II), especially that for the incoming but also that for the emerging particle, are large. Physically, this means that the projectile on entering the nucleus (after passing through or over the Coulomb barrier) is not likely to re-emerge in the same channel. Such a situation is easily visualized for compound projectiles, e.g., d, He^3, or H^3. Because of the strong nuclear absorption, it seems likely that the most important contributions to the stripping matrix elements arise from limited regions close to and particularly outside the nuclear surface.[33] This is especially valid if the captured particle(s) is(are) loosely bound. Thus, it can be argued that for such cases, only a limited band of angular momenta will contribute to the reaction matrix element.[47] Indeed, Goldfarb and Hooper[48] found that the main contribution to the overlap integral for deuteron stripping comes from a small band of angular momenta centered about a critical value L_c. The latter is related to an "interaction radius," R_c by $R_c\approx(L_c+1)\lambda\!\!\!^{-}$, where $\lambda\!\!\!^{-}$ is the reduced wavelength of the projectile. They attempt to understand the validity of the plane-wave Born approximation from this point of view. Similar conclusions have been drawn by Blair[49] for elastic and inelastic scatterings from deformed nuclei. We believe that these findings are not peculiar to the processes considered; they are rather expected to be characteristic of direct nuclear reactions initiated by compound particles in the intermediate energy region (10–50 MeV) if the emerging particle is also strongly absorbed.

There is another feature common to medium-energy nuclear reactions, namely, that a wave picture applies rather than a particle one. It is this property which allows one to draw on analogies to physical optics, and which leads one to expect interference and diffraction phenomena. The role of nuclear structure is to provide selection rules (e.g., angular momentum, parity) which are of particular interest for spectroscopic studies. These rules determine the shape and oscillations of the angular distribution superimposed on the gross diffrac-

[45] See also the comment made by G. R. Satchler, quoted by A. G. Blair and H. E. Wegner, Phys. Rev. **127**, 1233 (1962).

[46] B. G. Harvey, J. Cerny, R. H. Pehl, and E. Rivet, Nucl. Phys. **39**, 160 (1962).

[47] N. Austern, in *Proceedings of the Rutherford Jubilee International Conference, Manchester, 1961* (Academic Press Inc., New York, 1961), p. 462.

[48] L. J. B. Goldfarb and M. B. Hooper, Phys. Letters **4**, 148 (1963).

[49] J. S. Blair, Phys. Rev. **115**, 928 (1962).

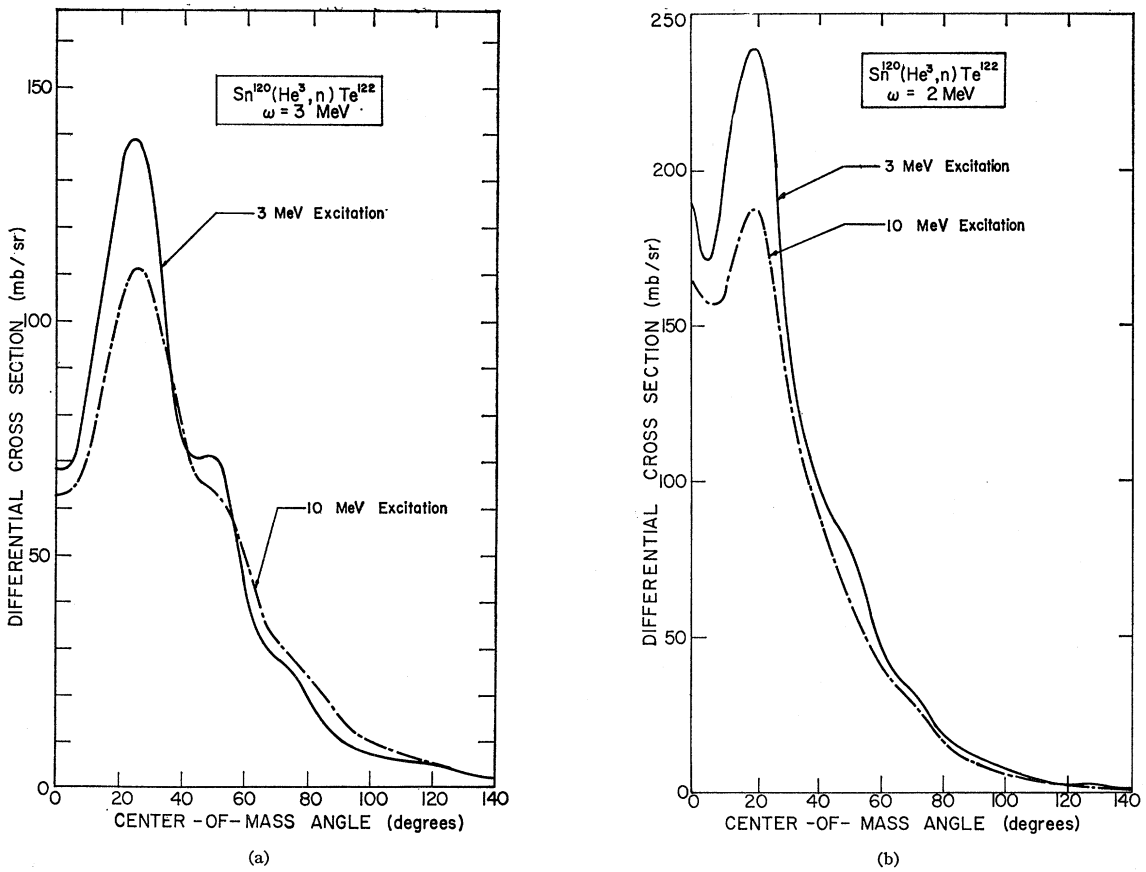

FIG. 15(a) and (b). Sum of cross sections for the $Sn^{120}(He^3,n)Te^{122}$ reaction. See Fig. 14 for data, except that $\omega=2$ MeV in Fig. 15(b).

tion patterns, and they influence the magnitude of the cross section. In the case of stripping reactions, it will be seen that the forward peak can be attributed mainly to optical interference, and details of the oscillations to this and to the nuclear structure effects.

We shall now develop a simple model for stripping when strong absorption occurs; for definiteness, again consider the (He^3,n) reaction.

A. Ring Model

First, in order to bring out the main ideas of this model, we make the following assumptions, which we will discuss and relax later on: (a) the outgoing neutron waves have a spherical "intrinsic radiation pattern;" (b) the diproton bound-state wave function is concentrated at the nuclear surface; (c) the stripping interaction has zero range; (d) the nuclear surface is sharp; (e) Coulomb effects are negligible.

Since the He^3 and n are strongly absorbed by the nucleus, we shall rely on a W.K.B. treatment[50] of the type suggested by Schiff[51] to describe the distorted waves. With assumptions (c), (d), and (e), the incident and final scattered wave functions can be represented by plane waves in the "allowed" regions.[52] With respect to the incident-beam direction, the only "forbidden" region for the He^3 is a semi-infinite cylinder of radius R_c behind the nucleus and closed by the spherical nuclear surface in front of the nucleus. Similarly for neutrons emitted at 0° the "forbidden" region is a cylinder of radius R_c in front of the nucleus and closed by the spherical cap behind the nucleus. These forbidden regions are shown in Fig. 18. At this angle, with assumption (b), the effective nuclear rim is confined to a narrow ring, the axis of which is parallel to the incoming beam. Realistically, this ring cannot be infinitely sharp. For neutron emission in directions somewhat away from 0° (i.e., $\theta\lesssim 30°$), interference still arises from a "fuzzy ring" region. Thus, we consider the ring to be the neutron source even for small nonzero scattering angles.[53] With assumptions (a) and (c), the cross section is pro-

[50] N. Austern, Ann. Phys. (N. Y.) **15**, 299 (1961); T. A. Eriksson and G. A. Rinander, Arkiv Fysik **24**, 1 (1963).
[51] L. I. Schiff, Phys. Rev. **103**, 446 (1956).
[52] See, for example, E. M. Henley, Nucl. Phys. **13**, 317 (1959).
[53] If one takes the ring too seriously and corrects for the direction of neutron emission, then one gets into the "crescent moon" difficulty discussed by J. S. Blair (Ref. 49). Our approximation gives more reasonable results. However, time reversal invariance is not preserved.

portional to D_J [see Eq. (42)] and can be written approximately (neglecting $A/A+2$) as

$$d\sigma/d\Omega \propto \sum_M \left| \int \chi_k^{-*}(\mathbf{R}) \phi_{NJ}{}^{M*}(\mathbf{R}) \chi_K^{+}(\mathbf{R}) d^3R \right|^2$$

$$\approx \sum_M \left| \int' e^{-i\mathbf{k}\cdot\mathbf{R}} \mathcal{R}_{NJ}(R) Y_J{}^{M*}(\theta_R, \varphi) e^{i\mathbf{K}\cdot\mathbf{R}} d^3R \right|^2, \quad (50)$$

where the prime on the last integral indicates that it is limited to the allowed regions discussed above. The only contribution to the matrix element, in our approximation, arises from the ring of radius R_c, over which $\mathbf{K}\cdot\mathbf{R}$ is constant. The problem is then akin to that of inelastic scattering,[49] and Eq. (50) becomes[54]

$$d\sigma/d\Omega \propto \sum_M \left| \int_0^{2\pi} d\varphi e^{-ikR_c \sin\theta \cos\varphi} Y_J{}^{M*}(\pi/2, \varphi) \right|^2,$$

where θ is the scattering angle. The integration is readily carried out, and we find

$$d\sigma/d\Omega \propto \sum_M |J_M(kR_c \sin\theta) \Theta_J{}^M(\tfrac{1}{2}\pi)|^2, \quad (51)$$

where $Y_J{}^M(\theta,\varphi) = (2\pi)^{-1/2} \exp(iM\varphi) \Theta_J{}^M(\theta)$. For an even-even target nucleus, the angular distribution for a transition to the ground state (or any $0 \rightarrow 0$ transition) is characterized by the cylindrical Bessel function (J_M) of zero order. This is also the angular distribution that would be obtained for a classical ring radiating neutrons in phase; for such a radiator the intensity is

$$I \propto \left| \int_0^{2\pi} d\varphi e^{ikR_c \sin\theta \cos\varphi} \right|^2 = 4\pi^2 J_0{}^2(kR_c \sin\theta). \quad (52)$$

The appearance of the cylindrical rather than the spherical Bessel function is not counter to experimental information.[55] The arguments of the Bessel functions in Eqs. (51) and (52) differ from that of the plane-wave Born approximation in that $|\mathbf{K}-\mathbf{k}|$ is replaced by $k \sin\theta$. Thus, for ground-state transitions, or in fact, any transitions characterized by $J=0$, Eq. (51) predicts an angular distribution peaked at 0°. This is shown in Fig. 16 where we take $kR_c=5$ for purpose of illustration.

For transitions characterized by $J \neq 0$, cylindrical Bessel functions of all even orders up to J appear in the angular distribution if J is even, whereas only odd ones occur if J is odd. The other terms vanish because $\Theta_J{}^M(\frac{1}{2}\pi)$ is zero unless $J-M$ is even. Since only the zero-order Bessel function does not vanish at 0°, the cross section to odd J states does not necessarily peak forwards. However, for even J states it tends to do so. This is brought out in Fig. 16 where we show the angular

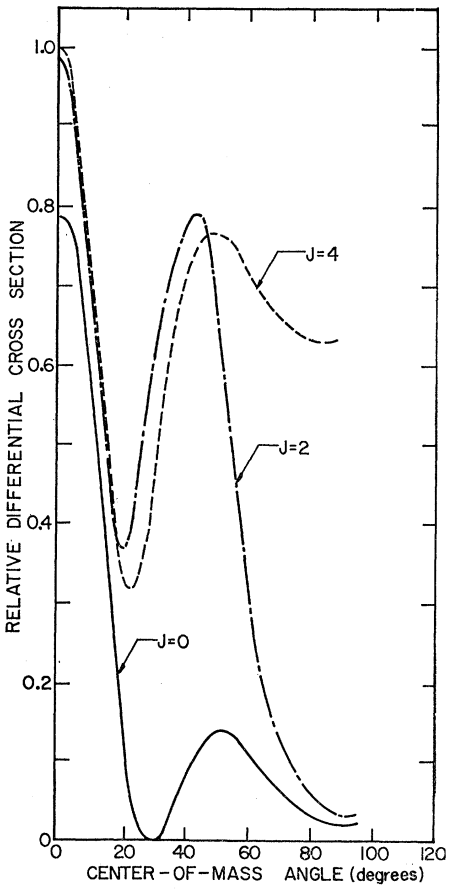

FIG. 16. Relative differential cross sections predicted by the ring model for excitation of 0^+, 2^+ or 4^+ states by a stripping reaction on an even-even target nucleus, with $kR_c=5$.

distribution given by Eq. (51) with $kR_c=5$ for $J=2$ and for $J=4$. By contrast, the angular distribution for excitation of odd parity states is zero at 0°. This does not agree with the distorted-wave calculation for C^{12} (cf. Fig. 3) and arises from the assumptions made in the ring model.

To compare with poor resolution experiments, the cross section must be summed over relevant final states. If the target nucleus is even-even and the two protons are captured into the same major shell, the selection rules only permit excitation of even ($J=$) J_f states. In Fig. 17 appear the angular distributions anticipated with this yet unimproved model for final states of $J_f=0$ only, $J_f=0$ and 2, and finally $J_f=0$, 2, and 4. For illustrative purposes, the spectroscopic weights and neutron wave number k are taken to be the same for all states. The latter is in the spirit of the adiabatic approximation.[49] It is seen that, in all cases, a strong forward peaking is predicted.

Before improving our model to compare it with experiments and the distorted-wave calculations, we shall discuss some of the approximations inherent in Eq. (51).

[54] This approximation remains valid even for a fuzzy ring as long as $\mathbf{K}\cdot\mathbf{R} \ll 1$.

[55] See, for example, O. M. Bilanuk and R. J. Slobodrian, Phys. Letters 4, 209 (1963).

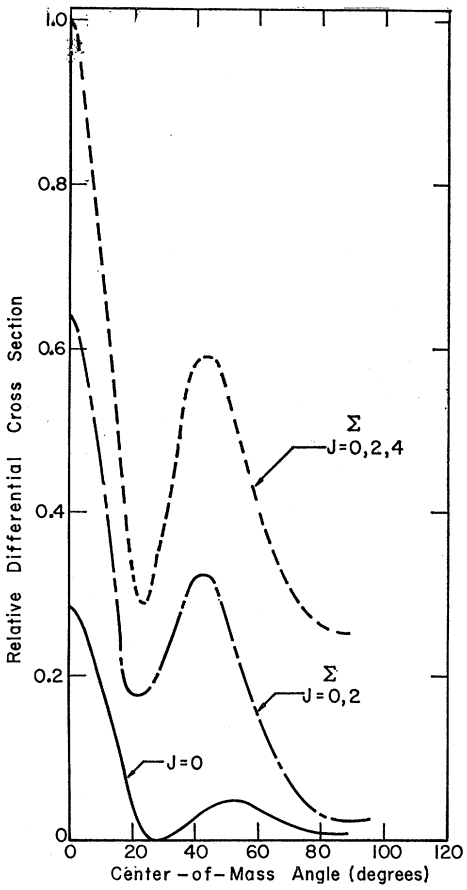

FIG. 17. Sums of differential cross sections shown in Fig. 16; the spectroscopic weights are taken to be the same for all states. The solid curve is for $J=0$ only, the dot-dash curve for the $J=0+J=2$ states, and the short dash curve for $J=0+J=2+J=4$ states.

Assumption (a) refers to an "intrinsic radiation pattern" of neutrons. We have given it this name because it corresponds to an assumption in the classical radiator model of Eq. (52). In this classical model a nonspherical radiation pattern would arise from the conservation of linear momentum and the internal structure of the He^3 nucleus. Its effect (if the radiation pattern is φ independent) is to simply multiply the angular distribution, Eq. (52), by a "form-factor envelope." The radiation pattern is then limited by the momenta available to the neutron and the modulation would be expected to be given by the Serber[2] stripping angular distribution, i.e., by the form factors discussed in Sec. IIA. As argued in that section and in Sec. IIC this form factor is almost constant, and therefore essentially irrelevant, in the region of scattering angles where the present model is applicable. How does such an "intrinsic radiation pattern" arise in the quantum-mechanical formulation that leads to Eq. (51)? It would appear if we used Eq. (36) for the distorted waves in the matrix $\mathfrak{M}_J$ of Eq. (34). However, it is no easier to justify the use of this equation here than in the optical-model description. Since the form-factor effect is small in any case, we shall not consider it further.

The relaxation of assumptions (b), (c), and (d) which we carry out in the shadow model described below, leads to a fuzzy, rather than to a sharp, ring. This has also been examined in the classical picture where the primary effect is to (slightly) fill in the minima of the angular distributions.

Since He^3 is a charged nucleus, its Coulomb interaction with the target may indirectly change the angular distribution of the neutrons. This has been neglected in the above model [assumption (e)]. Classically, the Coulomb trajectory of the He^3 preferentially tends to send off neutrons at angles other than 0°.[56] Since only a few angular momenta close to L_c are of importance, the classical picture may not be far amiss. If the intrinsic radiation pattern of the outgoing neutrons were sharp (i.e., of half-width $\lesssim 20°$), then the deflection of the incident He^3 by the Coulomb field of the target might indeed shift or change the angular distribution of neutrons at small angles. The effect is expected to be of order $V_c(R_c)/E=Zze^2/R_c$, where E is the energy of the incident projectile, of charge z, and V_c is the Coulomb energy at the critical radius R_c. However, we have already seen that the intrinsic radiation pattern is broad and that its effects are negligible for the energies and scattering angles we consider. We thus expect Coulomb effects to be small.

A similar argument can be made in a wave picture. The Coulomb potential causes a distortion of the wave and a reduction of the incident wave number. These both influence the neutron emission, but if $V_c(R_c)/E \ll 1$ (or if no intrinsic radiation pattern limitation is imposed) then the changes in the angular distribution are expected to be small. We are presently investigating Coulomb effects in more detail.

B. Cylindrical Shadow Model

The ring model is still rather crude, even though it qualitatively describes, for example, the (He^3,n) process. We now extend the model by removing some of the drastic assumptions in (A) and using a slightly more complicated, but also more realistic, description of the stripping reaction.

Again, we assume that for distances smaller than some critical radius R_c (not necessarily the same as for the ring model) of the target nucleus, the He^3 and neutron waves are completely absorbed. For 0° neutron emission an infinitely long cylindrical region of radius R_c is then cut out of the integration needed to find D_J (see Fig. 18). We still make this approximation for nonforward angles, but relax assumptions (b), (c), and (d) of the ring model; that is we no longer assume that the contribution to the matrix element comes from the nuclear surface. The integral to be evaluated is given by

[56] D. R. Inglis, Nucl. Phys. 44, 460 (1963).

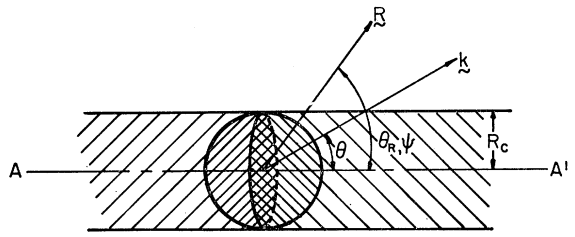

FIG. 18. Pictorial representation of the ring and shadow models. The direction of the incident beam is from A to A', that of the outgoing beam is along $\mathbf{k}$. The radius of the nucleus is R_c. The incident beam is assumed not to penetrate into the region with slanted lines of negative slope, whereas the shadow region for the outgoing particles is taken to be the region of lines with positive slope. The ring is the boundary of the crosshatched region.

the second form of Eq. (50); it is then no longer true that $\exp(i\mathbf{K}\cdot\mathbf{R})$ is constant. Since we are not interested in the nuclear interior, $\mathfrak{R}_{NJ}(R)$ can be approximately represented by its asymptotic form $[\exp(-\alpha' R)]/R$, the exponential falloff being characteristic of the eigenfunction in a finite well. The parameter α' is analogous to the strength constant of the simple harmonic oscillator considered in earlier sections.

Thus, choosing AA' as the polar axis (see Fig. 18) we have

$$\mathfrak{M}_J' = \mathfrak{R}_{NJ}(R_c)e^{\alpha' R_c}R_c\int_0^{\pi} d\theta_R Y_J{}^{M*}(\theta_R,\varphi) \times\sin\theta_R\int_0^{2\pi} d\varphi\int_{R_c\csc\theta_R}^{\infty} dRR \times e^{i[KR\cos\theta_R - kR(\cos\theta\cos\theta_R+\sin\theta\sin\theta_R\cos\varphi)]}e^{-\alpha' R}, \quad (53)$$

where we have normalized the bound-state wave function by fitting it onto the interior wave function. [For computational purposes $\mathfrak{R}_{NJ}(R_c)$ is taken to be the average of those for different J for the harmonic oscillator with $\omega=3$ MeV. Note that this is taken to be independent of J because we use the same exponential falloff for all these states.] The surface of the cylinder is bounded by $R\sin\theta_R = R_c$. Separating the spherical harmonics, we have

$$\mathfrak{M}_J' = (1/2\pi)^{1/2}\mathfrak{R}_{NJ}(R_c)e^{\alpha' R_c}R_c\int_0^{\pi} d\theta_R\Theta_J{}^M(\theta_R) \times\sin\theta_R\int_0^{2\pi} d\varphi e^{-iM\varphi}\int_{R_c\csc\theta_R}^{\infty} dRRe^{-R(y+iz\cos\varphi)}, \quad (54)$$

where $y=\alpha'-iK\cos\theta_R+ik\cos\theta\cos\theta_R$ and $z=k\sin\theta\sin\theta_R$. We first perform the radial integration,

$$\int_{R_c\csc\theta_R}^{\infty} dRRe^{-R(y+iz\cos\varphi)} = -\frac{\partial}{\partial y}\left[\frac{e^{-R_c\csc\theta_R(y+iz\cos\varphi)}}{y+iz\cos\varphi}\right].$$

At forward angles $|z|$ is much smaller than $|y|$, and we find

$$\mathfrak{M}_J' \approx (2\pi)^{1/2}\mathfrak{R}_{NJ}(R_c)e^{\alpha' R_c}R_cJ_M(kR_c\sin\theta) \times\left[\int_0^{\pi} d\theta_R\Theta_J{}^M(\theta_R)\frac{e^{-R_cy\csc\theta_R}}{y^2}(\sin\theta_R+R_cy)\right]. \quad (55)$$

The angular dependence of the cross section is thus again characterized by cylindrical Bessel functions of argument $kR_c\sin\theta$. The θ_R integral (which is evaluated numerically) gives rise to weighting factors for the various M substates; they depend on the scattering angle through y.

With $k\lesssim K$ and for $J=0$, Eq. (55) reduces to Eq. (51) to within a multiplicative constant. When α' is large, corresponding to a large binding energy, the shadow model gives almost identical results to those of the ring model for all J. As α' decreases, the ratio of the 0° flux of neutrons to that of the first finite angle maximum decreases (except for $J=0$), and the cross section at large angles is also reduced; however, our

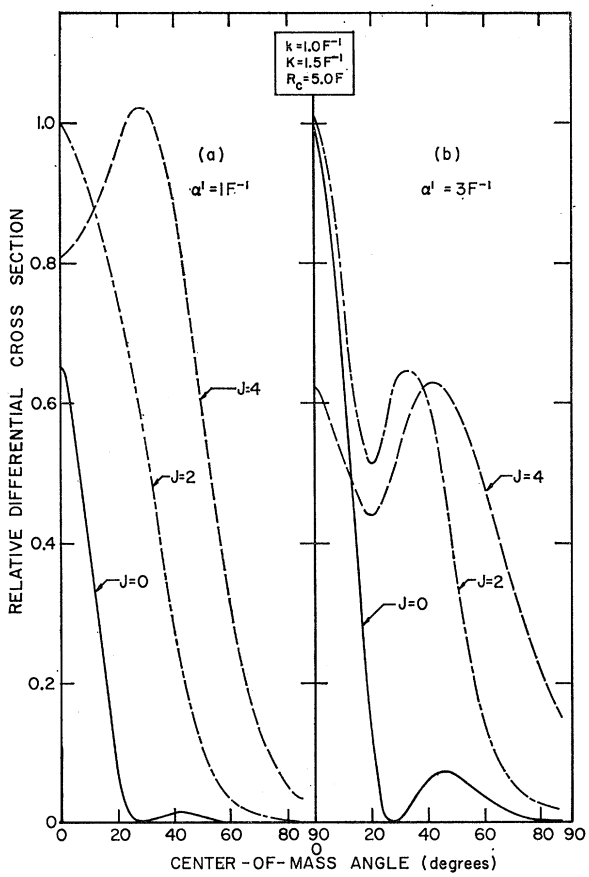

FIG. 19. Relative differential cross sections predicted by the shadow model for the excitation of 0^+, 2^+, or 4^+ states by a stripping reaction on a typical target nucleus. The wave numbers K and k refer to the incident projectile and outgoing particle, respectively. R_c is the "nuclear radius" and α'^{-1} is the characteristic fall-off distance of the bound-state wave function.

present model is inapplicable in this region. A generalization of it to such angles is presently being investigated.

In Figs. 19(a) and 19(b) relative differential cross sections to various final states are presented for $\alpha'=1$ F^{-1} and $\alpha'=3$ F^{-1}, respectively. The other parameters are chosen to be typical for medium-energy reactions on a target nucleus that is not too heavy: $W_J=1$, $K=1.5$ F^{-1}, $k=1$ F^{-1} for all final states, and $R=5$ F. For these parameters the angular variation is almost identical with that of the ring model if $\alpha'=6$ F^{-1}. With the method of normalization described in Eq. (53), the 0° cross section for the $J_f=0$ state is 3.8 mb/sr with $\alpha'=1$ F^{-1} and 0.3 mb/sr with $\alpha'=3$ F^{-1}. These cross sections are of the right order of magnitude. As α' decreases from 6 F^{-1} to 1 F^{-1}, the relative cross section to the 4^+ state appears to increase. However, with the above parameters, the excitation of the 4^+ state dominates for all α' larger than 1 F^{-1}. Comparison of Figs. 19(a) and 19(b) with Fig. 9 shows that our model is able to qualitatively reproduce the distorted-wave results. In particular, the sharp forward maximum of the $J_i=0$ to $J_f=0$ transition and the less strong forward peaking of the $J_i=0$ to $J_f=2$ transition is obtained. For the excitation of 4^+ states, the forward peaking is diminished by decreasing α'. The shadow model predicts deeper minima than the distorted-wave model; this undoubtedly arises from the use of our sharp cutoff.

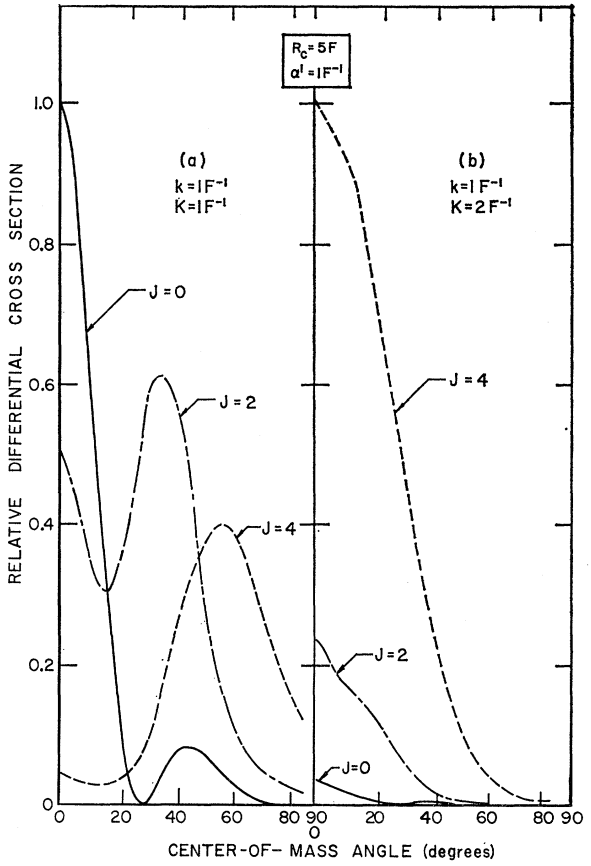

FIG. 20. Variation of differential cross sections with $|K-k|$ predicted by the shadow model. For notation, see Fig. 19.

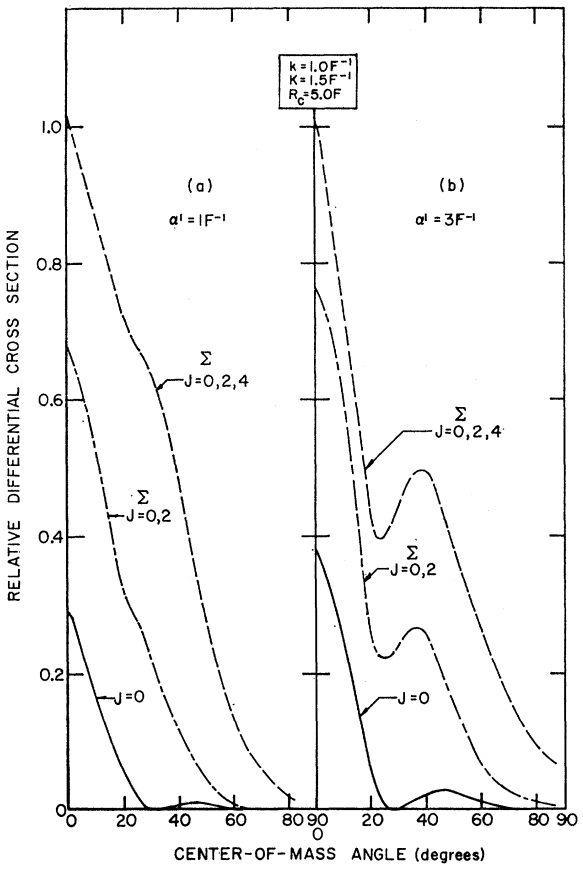

FIG. 21. Sums of differential cross sections shown in Fig. 19; equal spectroscopic weights are assumed for all states. The solid curve is for $J=0$ only, the dot-dash curve for the $J=0+J=2$ states, and the short dash curve for $J=0+J=2+J=4$ states.

The dependence of the differential cross section on $|K-k|$ can be deduced by comparing Figs. 19(a), 20(a), and 20(b). As this difference increases, the cross section to higher spin states is enhanced. A qualitative argument for this behavior is as follows.[45] Since the angular distribution tends to be peaked forward, the dominant angular momentum transfer is just $|K-k|R_c$; for then the incoming and outgoing wave oscillations tend to be in phase and thus have maximum overlap. A further feature to be noted is that for a fixed k, the diffraction minima tend to disappear as K increases.

In Figs. 21(a) and 21(b) appear the differential cross section predicted by Eq. (55) for the sum of various final states assumed to have (approximately) the same energy. The spectroscopic weight W_J is taken to be 1 for all of the relevant final states, and the sums of cross sections to the 0^+ and 2^+ as well as to the 0^+, 2^+, and 4^+ states are compared to the 0^+ states alone. Comparison with Figs. 12–15 again shows that the dominant

features of the distorted-wave theory and of experiment[43] are reproduced by our simple model. We believe (furthermore) that if one does not take all final states to be degenerate in summing cross sections, then the secondary maxima of Fig. 21 would tend to wash out.

Although we have not carried out a detailed investigation of the predictions of the cylindrical shadow model for the dependence of the differential cross section on the atomic weight of the target, we believe that the essential features of the distorted-wave theory will reappear here. That is, the angular distribution is expected to be relatively insensitive to A. The reasons are as follows. As the nuclear radius increases, so does the difference $|K-k|R_c$. The former sharpens the angular distribution for a given final state; this is also observed in the distorted-wave calculations (compare Figs. 9, 10, 11). In contrast, the increase of $|K-k|R_c$ tends to increase the magnitudes of the less forward peaked cross sections for the excitations of higher spin states. Although there is a broadening effect due to Coulomb distortions, we expect this to be small; this is also in agreement with our optical model calculations for which turning off the Coulomb interaction only causes a slight narrowing of the forward peak. Thus, when differential cross sections are summed over many final states, we anticipate its half-width at forward angles to be almost independent of A. This qualitative argument is not in disagreement with the results observed by Manley.[43]

V. CONCLUSIONS

We have used three approaches to discuss double stripping, with particular application to the (He^3,n) reaction.

The first of these is a plane-wave Born treatment. It predicts that the rapid angular variation of the differential cross section (characterized by the square of spherical Bessel functions) is modulated by a slowly varying form factor which decreases the back-angle yields. We have shown that, contrary to previous treatments, this form factor depends not only on the He^3 structure (e.g., radius), but also on the range and form of the stripping interaction. At medium energies, furthermore, the form factor is unimportant for forward angles ($\theta \lesssim 60°$). This approximation, with reasonable nuclear radii, is unable to explain the observed rapid variation of the differential cross sections at forward angles. Thus, two-nucleon stripping differs from deuteron stripping, in that the plane-wave Born approximation appears not to be useful for nuclear spectroscopic studies.

The second approach consists of a distorted-wave Born treatment. The reaction matrix element is derived without any zero-range approximations, by making use of infinite harmonic oscillator wave functions for the captured nucleons. However, in the actual numerical evaluation of this matrix, some range effects are neglected. Agreement with available experimental data is found to be excellent, without adjusting the optical-model parameters, but fixing the harmonic oscillator energy spacing so as to reproduce as closely as possible single-particle wave functions in a finite well outside the nucleus. For the energy chosen, it is shown that excitation of higher spin states ($J_f \approx 3$ or 4) is favored. When cross sections are summed over states obtained by filling the lowest available major shells, the angular distribution turns out to be strongly peaked at forward angles and has a half-width that is insensitive to the atomic weight A of the target. These characteristics can be understood qualitatively as follows: The nuclear distortion and absorption of the incident and outgoing waves cause the forward peaking; for a given final spin, the angular distribution becomes narrower with increasing A; however, differential cross sections for the excitation of higher spin states of the final nucleus are less peaked forwards than those of lower spin states, and these higher spin states increase in importance as A increases. Thus, the angular distribution for the sum of low-lying final states remains almost independent of A.

Finally, we have proposed a simple diffraction model which gives insight into the above features. This model presupposes strong absorption of the incident and outgoing particles by the respective nuclei. It is indeed able to reproduce the salient points of the distorted-wave theory and of experiment.

ACKNOWLEDGMENTS

We profited greatly from numerous valuable discussions with Dr. J. S. Blair, Dr. I. Halpern, and Dr. J. H. Manley; we also wish to thank the latter for making his data available to us prior to publication. In addition, we are grateful to T. G. Kelley and Dr. J. Wills for useful suggestions and some help with the numerical computations.